# *Ab initio* study of deformed As, Sb, and Bi with an application to thin films

M. Zouhar[1,*] and M. Šob[1,2,3,†]

[1]*Central European Institute of Technology, CEITEC MU, Masaryk University, Kamenice 5, CZ–625 00 Brno, Czech Republic*
[2]*Institute of Physics of Materials, Academy of Sciences of the Czech Republic, Žižkova 22, CZ–616 62 Brno, Czech Republic*
[3]*Department of Chemistry, Faculty of Science, Masaryk University, Kotlářská 2, CZ–611 37 Brno, Czech Republic*

(Received 3 August 2016; revised manuscript received 16 September 2016; published 28 November 2016)

We present a comprehensive density-functional theory study of total energy and structural properties of As, Sb, and Bi in their A7 ground-state structure and in the bcc, fcc, and simple cubic (sc) modifications. We also investigate continuous structural transitions between these structures. The electronic structures and total energies are calculated both within the generalized gradient approximation (GGA) and local-density approximation (LDA) to the exchange-correlation energy as well as with and without inclusion of the spin-orbit coupling (SOC). The total energies of deformed structures are displayed in contour plots as functions of selected structural parameters and/or atomic volume; these plots are then used for understanding and interpreting structural parameters of As, Sb and Bi thin films on various substrates. Our calculated values of lattice parameters for (0001) thin films of Bi on Si(111) and Ge(111) substrates agree very well with available experimental data. In analogy with that, we suggest to investigate (0001) thin films of As on Ti(0001), Co(0001), Zn(0001) and Rh(111) substrates, of Sb on C(0001), Zn(0001), Al(111), Ag(111) and Au(111) substrates and of Bi on Co(0001), Al(111), Rh(111), Ba(111) and Pb(111) substrates. For these cases, we also predict the lattice parameters of the films. A large part of our results are theoretical predictions which may motivate experimentalists for a deeper study of these systems.

DOI: 10.1103/PhysRevB.94.184110

## I. INTRODUCTION

The elements of the 15th group, As, Sb, and Bi, have received a great deal of attention, mostly due to many practical applications, especially in electronic devices. This has motivated a plethora of both experimental and theoretical studies of these elements [1–4] and corresponding thin films on various substrates, in particular of Bi on Si [5–12], Ge [13], and Rh [14].

Physical properties of thin (semi)metal films may differ from those of ground-state bulk materials because of structure changes and/or size effects as discussed, e.g., in Ref. [6], examining electronic properties of ultrathin Bi films on Si. Therefore studies of thin films of these elements are of high importance.

A possibility of producing a free-standing film grown on a subsequently removed substrate [15] can also be regarded as a motivation for a rather generally oriented study of thin films, i.e., without considering a specific substrate. Moreover, influence of the substrate is sometimes neglected, which is a natural simplification, in particular if the substrate and overlayer interact weakly, as mentioned, e.g., in Ref. [6] and references therein. Hence studies of free-standing films, examined, e.g., in Ref. [3], are also useful.

Experimental studies indicate that the [0001] or [111] directions are frequently encountered orientations of thin films grown on various substrates, in particular on those with a threefold symmetry, assuming the coverage is sufficiently high. For example, Ref. [16] reports a surface reorientation of thin Bi film that grows on Si(111) substrate. The lower-coverage films exhibit a so-called pseudocubic configuration with the $[110]_{\mathrm{rh}}$ (rhombohedral) orientation. However, the Bi[0001] axis becomes perpendicular to the Si(111) substrate at about 7-monolayer coverage. Such an orientation implies that the higher-coverage films can be well described with the help of trigonally deformed A7 rhombohedral unit cell (together with relaxation of the internal structural parameter $u$).

The above-mentioned orientations are not the only ones observed in experiment. For example, 30-nm Bi/Si(111) configuration investigated in Ref. [10] exhibits several peaks in the x-ray diffraction spectra (shown in their Fig. 2) and $(110)_{\mathrm{rh}}$ rhombohedral orientation is dominant. Such a film, however, cannot be reliably described using the trigonal structures studied in this work.

It turns out that the A7 ground-state structure of As, Sb, and Bi is very closely connected with the simple cubic (sc) structure. The sc structure appears in As under pressure [17] and the experimental values of structural parameters $c/a$ and $u$ of As, Sb, and Bi ground-state structures are not very far from those of the sc structure. Indeed, comparison of the corresponding A7 ground state values of $c/a$ and $u$ in Table I with those of sc structure ($u = 0.25$ and $c/a = \sqrt{6} \doteq 2.45$, see also Table II) shows that the relative differences for these two parameters are 13%, respectively 9%, in case of As ground state, which deviates from the sc structure the most. The structural transformations from A7 to sc structure were studied in As both experimentally [17] and theoretically [18–22].

If we apply an increasing pressure to As, Sb, and Bi, the A7 structure undergoes a transformation—over some intermediate structures—to the body centered cubic (bcc) structure. This transformation has also been studied both experimentally [23–25] and theoretically [26,27]; a review is provided in Ref. [28]. However, to the best of our knowledge, a detailed comparative study of energetics of these elements in all the A7, bcc, sc, and fcc structures, with application to thin films, is still missing.

The purpose of this paper is to fill in this gap. We present a detailed and comprehensive analysis of the total energy behavior of As, Sb, and Bi in a three-dimensional

*sybok@physics.muni.cz; Present address: Xura, Inc., Holandská 5, CZ-639 00 Brno, Czech Republic.
†sob@chemi.muni.cz

 

TABLE I. Lattice parameters $a$ and $c$ in hexagonal notation as well as the internal parameter $u$ of As, Sb, and Bi in the A7 crystal structure at 4.2 K [1,2] (see also Fig. 1). The rhombohedral lattice parameter $a_{\rm rh}$, the rhombohedral angle $\alpha_{\rm rh}$ and the atomic volume $V_{\rm exp}$ are also given.

| | $a$ (Å) | $c$ (Å) | $u$ | $c/a$ | $a_{\rm rh}$ (Å) | $\alpha_{\rm rh}$ (°) | $V_{\rm exp}$ (Å$^3$/at) |
|---|---|---|---|---|---|---|---|
| As | 3.7597 | 10.4412 | 0.2276 | 2.7770 | 4.1018 | 54.55 | 21.30 |
| Sb | 4.3007 | 11.2220 | 0.2336 | 2.6093 | 4.4898 | 57.23 | 29.96 |
| Bi | 4.5330 | 11.7970 | 0.2341 | 2.6025 | 4.7236 | 57.35 | 34.99 |

parameter space spanned by the volume per atom, trigonal distortion (equivalent to the rhombohedral angle) and an internal structural parameter $u$ [29] that describes grouping (nonequidistance) of atomic planes along the [0001] direction into bilayers. And, indeed, it was demonstrated that thin films of Bi may grow in a bilayer mode [11] depending on the experimental conditions and substrate.

For graphical presentation of the results, we choose two-dimensional subspaces so that each of them includes at least two high-symmetry cubic structures or the ground-state A7 structure and cubic allotrope. The corresponding two-dimensional contour plots are then used to analyze and predict the structural parameters of As, Sb, and Bi thin films on various substrates in a similar spirit as in previous studies of Fe, Co, and Ni [30–32].

The paper is organized as follows. After providing computational details in Sec. II, Sec. III exhibits equilibrium parameters of all three basic cubic and A7 structures and energy contour plots for the paths connecting basic cubic structures along trigonal deformation as well as those connecting the bcc, A7, and fcc structures. Calculated contour plots are then used to determine the interlayer distances of Bi thin films on Si(111) and Ge(111). Encouraged by a good agreement with available experimental data, consisting in most cases only of values of lattice parameters $c$ and $a$, we provide plenty of predictions of structural parameters of epitaxial thin films of As, Sb, and Bi on various substrates. Section IV then briefly summarizes the results and provides conclusions.

TABLE II. Some characteristics of cubic structures expressed in the hexagonal notation of A7 structure (first three numerical columns, cf. also Fig. 1), and in an alternate notation of Ref. [34] (last two numerical columns). The value of $r_{c/a}$ is defined as $r_{c/a} = [\ln(c/a) - \ln(c/a)_{\rm sc}]/\ln 2$. The relation between rhombohedral angle $\alpha_{\rm rh}$ and $c/a$ is given in the equation (1). Reference [34] employs a different scaling of $c/a$ and a different rhombohedral angle (denoted here as $\tilde{\alpha}_{\rm rh}$) which, in case of A7 structures, corresponds to a face-centered rhombohedral cell with 8 atoms per cell [35]. The quantity $\tilde{c}/a = 2u\,c/a$ represents the $c/a$ ratio for the blue rhombohedral-like structure in the middle panel of Fig. 1. For comparison, the last line exhibits average values of these parameters in experimentally found As, Sb, and Bi A7 structures.

| | $u$ | $c/a$ | $\alpha_{\rm rh}$ (°) | $r_{c/a}$ | $\tilde{c}/a$ | $c/a$[a] | $\tilde{\alpha}_{\rm rh}$ (°)[a] |
|---|---|---|---|---|---|---|---|
| bcc | 0.25 | $\sqrt{6}/2 \doteq 1.22$ | 90.00 | $-1$ | $\sqrt{6}/4$ | 1 | 109.47 |
| sc | 0.25 | $\sqrt{6} \doteq 2.45$ | 60.00 | 0 | $\sqrt{6}/2$ | 2 | 90.00 |
| fcc | 0.25 | $2\sqrt{6} \doteq 4.90$ | 33.56 | 1 | $\sqrt{6}$ | 4 | 60.00 |
| A7 | ≈0.23 | ≈2.6 | ≈56 | ≈0.1 | ≈1.2 | ≈2.1 | ≈87 |

[a]Reference [34].

## II. COMPUTATIONAL DETAILS

The bulk ground-state structure of the elements As, Sb, and Bi is the rhombohedral A7 structure [1,33] (space group No. 166 ($R\bar{3}m$), Pearson symbol hR2) and it may be characterized by three parameters—hexagonal lattice constants $a$ and $c$ and an internal parameter $u$. Equivalently, rhombohedral lattice parameter $a_{\rm rh}$ and angle $\alpha_{\rm rh}$ may be used instead of $a$ and $c$ (Fig. 1). Relations among these equivalent sets of parameters are as follows:

$$\cos\alpha_{\rm rh} = \frac{(c/a)^2 - \frac{3}{2}}{(c/a)^2 + 3}, \quad a_{\rm rh} = \frac{1}{3}\sqrt{3a^2 + c^2}. \tag{1}$$

The structural parameters relate to the first and second nearest neighbor distances $l_1$ (corresponding to the shortest distance of one atom from layer "A" and one from layer "c" in Fig. 1) and $l_2$ (layers "c" and "B" in Fig. 1) as follows:

$$l_n(u) = \sqrt{\frac{a^2}{3} + \frac{c^2}{9}(n - 6u)^2}, \quad n \in \{1,2\}. \tag{2}$$

Taking the experimental lattice parameters of the A7 ground-state structure of Bi (Table I), the above formula yields $l_1 = 3.063$ Å and $l_2 = 3.512$ Å. It may be easily seen that $l_1(0.25) = l_2(0.25)$. The distances between atomic layers $d_{\rm c-B}$ (layers c and B in Fig. 1) and $d_{\rm A-c}$ (layers A and c in Fig. 1) differ by $(1 - 4u)c$.

Thus we see that the internal parameter $u$ is related to the spacing of the (0001) atomic layers and degeneracy of nearest neighbor distances. If $u \neq 0.25$, these atomic planes are not equidistant and form bilayers (Fig. 1). On the other hand, if $u = 0.25$, then the atomic planes along (0001) are equidistant and some of the interatomic distances coincide. For all three elements studied here, the values of $u$ are close to 0.23 (Table I).

The ground-state A7 structure is also referred as pseudo-cubic because it may be obtained, by small distortions along the (111) direction, from the simple cubic (sc) structure, which exhibits the parameters $u = 0.25, \alpha_{\rm rh} = 60°$ and the lattice constant $a_{\rm sc} = a_{\rm rh}/\sqrt{2}$ (Fig. 2). Thus, in some cases, we may approximate the ground-state structure of these elements by the sc structure. Of course, it has to be verified whether this approximation is reasonable in a study of a particular problem.

The correspondence between the rhombohedral (rh) [36] and hexagonal (hex) indexing system used by other authors [7,10,16] is as follows:

$$\begin{aligned}
[0001]_{\rm hex} &= [111]_{\rm rh},\\
(0001)_{\rm hex} &= (111)_{\rm rh},\\
(01\bar{1}1)_{\rm hex} &= (110)_{\rm rh},\\
(10\bar{1}1)_{\rm hex} &= (100)_{\rm rh}.
\end{aligned} \tag{3}$$

In the following text, the explicit marking hex of hexagonal system is suppressed. The [0001] axis corresponds to body diagonal of the distorted cubic lattice.

In this paper, we will describe the structures studied by means of the parameters $V/V_{\rm exp}$, $c/a$ and $u$. Here $V$ denotes

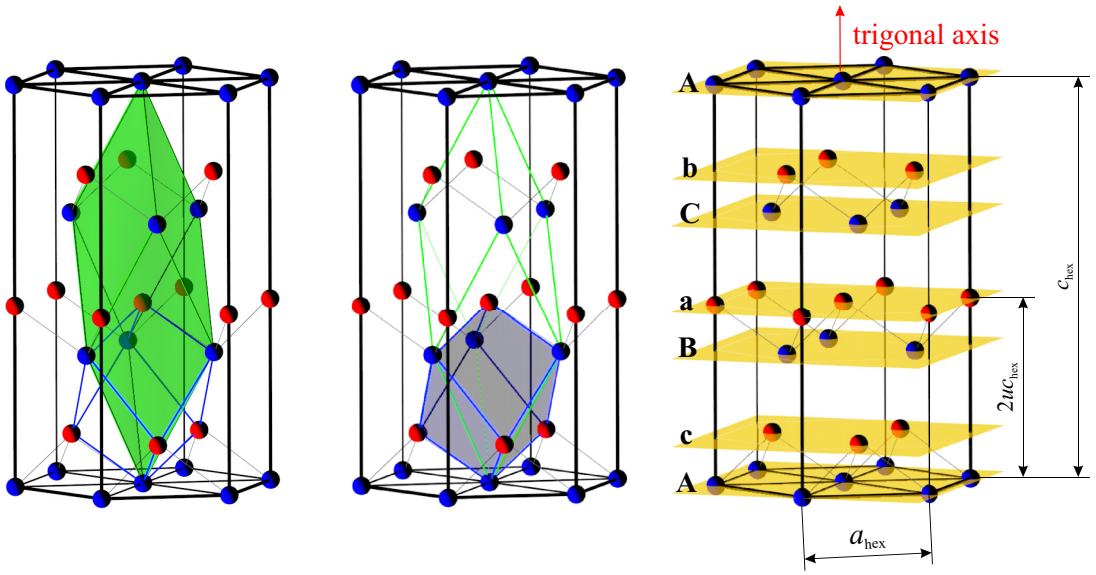


FIG. 1. A7 structure corresponding to the parameters $c/a = 3.11$ and $u = 0.225$. The parameters were chosen such as to demonstrate clearly the differences between a general A7 structure and the sc structure presented in Fig. 2. All three panels of this figure show the hexagonal envelope. The left panel also includes the rhombohedral cell (green) with rhombohedral angle $\alpha_{rh} = 49.8^\circ$ and the middle one shows an sc-like deformed body (blue) which, however, is not a rhomboeder in case of a general A7 structure. The stacking of the atomic planes (exhibited in the right panel) is A, B, and C intertwinned with atomic planes a, b, and c shifted by $2uc_{hex}$. On the basis of that, the A7 structure can be represented by two fcc lattices shifted by $2uc_{hex}$ along trigonal axis.

the atomic volume (i.e. the volume corresponding to one atom in a structure), $V_{exp}$ is the experimental atomic volume in the A7 structure, $a$ and $c$ denote the lattice parameters in the hexagonal notation (Table I, Fig. 1) and $u$ is the internal structural parameter characterizing mutual position of atomic planes along the [0001] or [111] direction (cf. Fig. 1, $u \neq 0.25$, and Fig. 2, $u = 0.25$).

Setting $u = 0.25$ restricts the structures, that can be described using the remaining parameters, to basic cubic structures (bcc, sc, and fcc) and to the structures obtained by their trigonal deformation (uniaxial tension or compression along the [111] axis). The $u = 0.25$ subset is denoted by a line formed by squares in Fig. 3 depicting the $(c/a,u)$ plane at a constant atomic volume. This line represents a continuous path connecting all three basic cubic structures and it is often called trigonal deformation path. Fig. 3 also exhibits the transformation paths between the A7 and basic cubic structures; they are described in detail later. Let us note that here we use a normalized logarithmic quantity $r_{c/a} = [\ln(c/a) - \ln(c/a)_{sc}]/\ln 2$ instead of $c/a$; for cubic structures, it is given, together with other parameters, in Table II.

In previous papers [34,37–40], the trigonal deformation path was characterized by a parameter $c/a$, where $c$ is

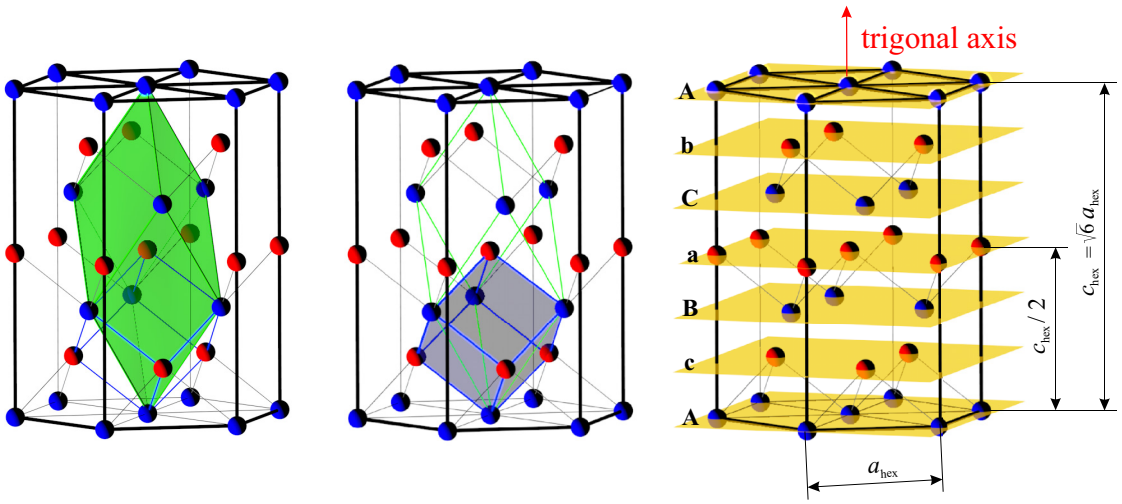


FIG. 2. A7 structure with parameters corresponding to the sc structure, i.e., $c/a = \sqrt{6}$ and $u = 0.25$ (see the description of Fig. 1 for further details). Let us note that the choice of $u = 0.25$ implies that the atomic planes are equidistant and no bilayers are formed. The blue body in the middle panel represents a unit cell of the sc structure.

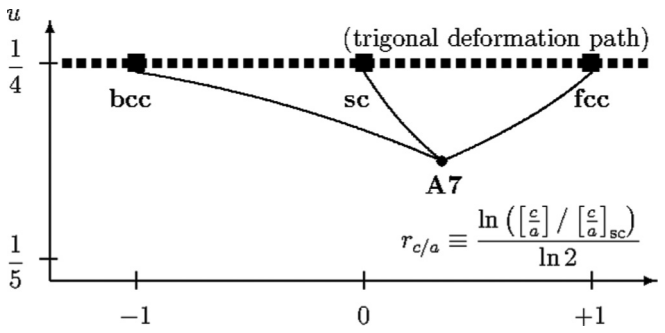


FIG. 3. The $(r_{c/a},u)$ plane in $(V,r_{c/a},u)$ parameter space. The cubic structures, connected by the trigonal deformation path, are marked by larger squares and the A7 structure corresponding to the values of $c/a = 3.11$ ($r_{c/a} \doteq 0.34$) and $u = 0.225$ as in Fig. 1 is marked by a dot. The paths joining the equilibrium A7 structure with one of the cubic structures are discussed in detail in the text and, for Sb, exhibited also in Fig. 4. They are straight lines in the $(c/a,u)$ plane, but here they are represented by curves because we display them in the plane $(r_{c/a},a)$.

measured along the [111] direction and $a$ is measured along a perpendicular direction. If we ascribe the value of $c/a = 1$ to the bcc structure, then at $c/a = 2$ we obtain the sc structure and at $c/a = 4$ the fcc structure; all other structures along the path are trigonal. In the following, we will refer to this scaling as to "1-2-4" notation.

In any scaling, the values of $c/a$ for the basic cubic structures satisfy

$$\left(\frac{c}{a}\right)_{\text{fcc}} = 2\left(\frac{c}{a}\right)_{\text{sc}} = 4\left(\frac{c}{a}\right)_{\text{bcc}}. \tag{4}$$

These three structures represent the only higher-symmetry structures encountered along the trigonal deformation path. It turns out that the derivative of the total energy with respect to the parameter describing the path is zero at these points, hence the total energy exhibits so-called symmetry-dictated stationary points, mostly minima or maxima [37,41]. Of course, other stationary points, not dictated by symmetry, may occur; they reflect properties of a specific material under study.

There are several alternate descriptions of the structures along the bcc-sc-fcc trigonal deformation path including one with two atoms in the basis with the atoms mutually shifted along the trigonal axis by $0.5c$. This description naturally includes the A7 structures because the numerical prefactor at $c$ in the shift stands for $2u$ (see Fig. 1) which, in case of structures at the trigonal deformation path, including the cubic structures, has a particular value of 0.5. This means both A7 and cubic structures can be joined by a path in a two-parameter plane $(c/a,u)$.

Let us note that the structures with $u = 0.25$ encountered along the trigonal deformation path (except for higher-symmetry bcc, sc, and fcc structures) do not exhibit any higher symmetry than the A7 structures with $u \neq 0.25$. Their Pearson symbol is hR1 and Strukturbericht notation is $A_i$ (usually for the structures between the bcc and sc structures) and A10 (usually for the structures between the sc and fcc structures), but their space group is the same as that of the A7 structures, i.e., $R\bar{3}m$ (No. 166). Therefore, indeed, except for the bcc, sc, and fcc structures, all the structures in the $(c/a,u)$ plane have the same space group.

The total energy calculations have been performed with the help of the VASP code using PAW potentials [42,43]. The exchange-correlation energy was treated using both LDA [44] and GGA-PW91 [45], with 670 k-points in the irreducible Brillouin zone sampled using the Monkhorst-Pack method. We have used an energy cutoff equal to 270 eV.

It has been demonstrated quite early that inclusion of spin-orbit-coupling (SOC) may be necessary, in particular for Bi, in order to achieve a better agreement of theoretical calculations with experiment [4]. That is why we perform the LDA and GGA calculations both without and with SOC.

All structures considered here are described by means of a hexagonal unit cell (see Figs. 1 and 2, the latter exhibiting the sc structure in this representation). The number of $k$ points based on convergence tests is sufficient for a well-converged total energy differences in case of all three elements considered. The error in calculated total energies may be estimated to be less than $5 \times 10^{-5}$eV/atom.

To get a deeper insight into the behavior of total energy, we analyze its course along the suitably chosen deformation paths. They are defined by a particular choice of the relation between $u$ and $c/a$. We may also change the volume along each deformation path and, in this way, we obtain two-dimensional profiles of the total energy in the subspace $[V/V_{\text{exp}},u(c/a)]$. The deformation paths $u(c/a)$ are selected as follows.

(1) bcc-sc-fcc (BSF-lin). This is the trigonal deformation path of cubic structures with constant $u(c/a) = 0.25$ discussed earlier.

(2) A7-simple cubic (AS-lin). Here, $u(c/a)$ is a linear function.

(3) bcc-A7-fcc (BAF-lin). In this case, we employ two different linear functions $u(c/a)$ for the segments bcc-A7 and A7-fcc.

(4) bcc-A7-fcc (BAF-cub). Here, $u(c/a)$ is a cubic polynomial with a minimum at the A7 structure.

The latter choice is motivated by the fact that this curve may be regarded to be closer to the minimum energy path connecting the bcc, A7, and fcc structures. The abbreviated description of the paths in the round brackets is based on the first letters designating the structures considered and have a suffix "-lin" (linear) or "-cub" (cubic) reflecting order of the polynomial function $u(c/a)$.

We consequently obtain variable volume total energy profiles by following such a path in the $(c/a,u)$ plane and by allowing for a volume change at each point on the path. Volume per atom is kept constant along each individual path. Set of these paths for different volumes gives the variable volume total energy profiles. The total energy contour plots display the results of exact DFT calculations on a rectangular grid. Each of the grid used (SA-lin, BA-lin, AF-lin (hence also BAF-lin), BAF-cub and that one for $(c/a,u)$ plane) contains at least 2150 DFT data points. To get equilibrium structures, the parameters $a$, $c/a$ and $u$ are fully relaxed. All other calculations are static with structural parameters being determined by the position of the structure on a selected deformation path.

The ranges of volume studied depend on element and approximation used but interval $V/V_{\text{exp}} \in [0.830,1.010]$ is

TABLE III. Calculated equilibrium structural parameters of As, Sb, and Bi in the A7 and cubic structures. The unlabelled values represent the ratio $V_{eq}/V_{exp}$ of calculated equilibrium atomic volume $V_{eq}$ and the experimental atomic volume in the A7 structure $V_{exp}$ and, in parentheses, the structural energy differences $E - E_{A7,\,eq}$ (meV/at) are given.

| | Structure | LDA | +SOC | GGA | +SOC | Others | | |
|---|---|---|---|---|---|---|---|---|
| As | A7 | 0.959 (0) | 0.960 (0) | 1.068 (0) | 1.068 (0) | 0.915 (LDA)[a] | 1.048 (PBE)[a] | 1.018 (PBE)[b] |
| | $a$ (Å) | 3.767 | 3.768 | 3.816 | 3.819 | 3.717 | 3.801 | 3.740 |
| | $c$ (Å) | 9.975 | 9.981 | 10.826 | 10.809 | 9.776 | 10.705 | 10.744 |
| | $u$ | 0.231 | 0.231 | 0.226 | 0.226 | 0.231 | 0.227 | 0.225 |
| Sb | A7 | 0.975 (0) | 0.977 (0) | 1.062 (0) | 1.066 (0) | 0.973 (LDA)[c] | 1.060 (GGA)[c] | 1.006 (LDA)[d] |
| | $a$ (Å) | 4.301 | 4.304 | 4.379 | 4.384 | 4.300 | 4.378 | 4.383 |
| | $c$ (Å) | 10.935 | 10.953 | 11.498 | 11.512 | 10.925 | 11.474 | 10.870 |
| | $u$ | 0.237 | 0.237 | 0.233 | 0.233 | 0.237 | 0.233 | 0.233 |
| Bi | A7 | 0.960 (0) | 0.987 (0) | 1.053 (0) | 1.089 (0) | 0.959 (LDA)[e] | 0.987 (LDA+SOC)[e] | 0.915 (LDA)[f] |
| | $a$ (Å) | 4.502 | 4.544 | 4.585 | 4.643 | 4.474 | 4.521 | 4.455 |
| | $c$ [Å] | 11.483 | 11.588 | 12.142 | 12.245 | 11.608 | 11.706 | 11.180 |
| | $u$ | 0.238 | 0.236 | 0.234 | 0.233 | 0.236 | 0.234 | 0.238 |
| As | sc | 0.900 (69) | 0.901 (69) | 0.960 (115) | 0.961 (115) | 0.859 (LDA)[a] | 0.944 (PBE)[a] | 0.904 (LDA)[g] |
| | bcc | 0.841 (383) | 0.841 (383) | 0.901 (454) | 0.901 (453) | | | 0.815 (LDA)[g] |
| | fcc | 0.854 (498) | 0.854 (497) | 0.914 (560) | 0.915 (559) | | | 0.825 (LDA)[g] |
| Sb | sc | 0.942 (22) | 0.944 (22) | 1.003 (45) | 1.006 (46) | | | |
| | bcc | 0.852 (186) | 0.854 (185) | 0.911 (244) | 0.914 (244) | | | |
| | fcc | 0.861 (281) | 0.863 (276) | 0.921 (333) | 0.923 (328) | | | |
| Bi | sc | 0.937 (22) | 0.958 (29) | 1.005 (40) | 1.035 (48) | | | |
| | bcc | 0.839 (89) | 0.860 (89) | 0.903 (139) | 0.932 (137) | 0.883 (PBE)[h] | 0.909 (PBE+SOC)[h] | |
| | fcc | 0.845 (151) | 0.866 (117) | 0.911 (194) | 0.941 (158) | | | |

[a]Reference [21].
[b]Reference [20].
[c]Reference [47].
[d]Reference [49].
[e]Reference [48].
[f]Reference [4].
[g]Reference [46].
[h]Reference [50].

covered in all the cases, where $V_{exp}$ is the experimental volume per atom given in Table I. In the case of As, Ref. [17] provides an empirical $u(c/a)$ A7-sc path that the structure undergoes under pressure, so that atomic volume is also changed here. For As, Sb, and Bi, similar paths can also be constructed to connect the A7 structure and observed bcc structure (found under pressure) but their endpoints are connected by complex host-guest structures [24] modeling of which is beyond the scope of this work. However, the paths described above may be applied to all elements studied and it is considerably easier to set up the calculations.

In the following, we strictly use the hexagonal cell and coordinates corresponding to the A7-rhombohedra (i.e., the green rhombohedra exhibited in the left part of Figs. 1 and 2). For cubic structures, the $c/a$ employed here is by factor of $\sqrt{6}/2$ larger than that employed in Refs. [34,37–39].

## III. RESULTS AND DISCUSSION

### A. Equilibrium structural parameters of A7, bcc, sc, and fcc structures

Calculated equilibrium structural parameters of As, Sb, and Bi in A7 structure as well as the atomic volumes of the cubic structures and structural energy differences determined in various approximations are given in Table III. For comparison, the Table also contains some DFT results of other authors. Experimental lattice parameters are given in Table I.

Let us discuss our structural parameters of the A7 structures first. When compared to the DFT results of other authors, relative differences are few percents; this is a very good agreement. The best agreement with experimental equilibrium volume is achieved within LDA+SOC approach, similarly as in earlier studies of Po [34,39]. Therefore our contour plots display predominantly the LDA+SOC results.

The inclusion of SOC leads to an increased equilibrium volume. Thus the approximations considered can be ordered, from the lowest to the highest equilibrium volume, as LDA, LDA+SOC, GGA, and GGA+SOC. Of course, the effects of SOC are diminished as the atomic number of the element decreases (i.e., in Sb and, in particular in As, the influence of SOC is much weaker).

Our LDA values of equilibrium volume of cubic structures of As are slightly larger (up to 3.5% of the experimental volume) than those of Ref. [46] and agree better with theoretical values exhibited in the overview Table III in Ref. [46]. Let us note that the overview Table II of lattice parameters of As in the sc structure provided in Ref. [21]

shows much larger differences in LDA-calculated equilibrium volumes—the scatter of the reported values is almost 20% (ranging from 0.86 to 1.05 measured in units of the equilibrium ground-state volume).

Comparing our results for the lattice constants of Sb with the values given in Ref. [47], we see a good agreement. Moreover, our LDA equilibrium volumes agree better with experiment than the GGA ones; the differences are only 3% in case of LDA and 6% in case of GGA.

The effect of SOC is most pronounced in case of Bi. Comparing our LDA and LDA+SOC values of equilibrium volume with those from Ref. [48], both our values are slightly lower, approximately by 3%. However, due to inclusion of SOC, our value of equilibrium volume increases by approx. 2.7%, which is in excellent agreement with Ref. [48] reporting also an increase of equilibrium volume of approx. 2.7% w.r.t. value without SOC in case of the A7 structure.

Our zero pressure volumes of sc and bcc structures calculated within the GGA agree very well with the corresponding ratios $(V/V_{\mathrm{A7,\,theor}})$ in Ref. [26]. Namely, when recalculated to the theoretical A7 volume, our volume ratios $V/V_{\mathrm{A7,\,theor}}$ for As, Sb and Bi for the sc and bcc structures from Table III give 0.90, 0.95, and 0.95 (sc structure) and 0.84, 0.86, and 0.86 (bcc structure), respectively. The corresponding values estimated from Fig. 3 in Ref. [26] amount to 0.90, 0.95, and 0.95 in case of the sc structure and 0.85, 0.86, and 0.86 in case of the bcc structure, respectively.

### B. Deformation paths with a fixed volume

Figure 4 exhibits the behavior of total energy of Sb in the $(c/a,u)$ plane at the equilibrium atomic volume of the A7 structure, $V/V_{\mathrm{exp}} = 0.977$. Here we may also see the deformation paths defined at the end of Sec. II: the standard trigonal deformation path, denoted also as BSF-lin (squares), three linear segments connecting the bcc-A7, sc-A7, and fcc-A7 structures (triangles) and a cubic path between the bcc, A7, and fcc structures (circles). Figure 5 shows then energy profiles of Sb as functions of $c/a$ along the trigonal deformation path for various volumes and as a function of $u$ for bcc, sc, and fcc structures.

In Fig. 4, we may observe saddle points corresponding to bcc and sc structures. As it follows from Fig. 5, there is an inflexion point with essentially zero derivative of energy with respect to $r_{c/a}$ at the fcc structure for $V/V_{\mathrm{exp}} = 0.977$. With respect to $u$, all these stationary points are maxima (see insets in Fig. 5). These three points (corresponding to the bcc, sc and fcc structures) are symmetry-dictated stationary points [34,37,41]. The maximum close to the bcc structure, the minima accompanying the fcc structure as well as the minima close to sc structure representing the equilibrium A7 structure (Fig. 4) are not dictated by symmetry and their presence (at the atomic volumes examined) characterizes the system under study, i.e., Sb in the present case. Also the saddle point located at $(c/a,u) \approx (1.56,0.22)$ (with $r_{c/a} \approx -0.65$) is not dictated by symmetry. As it is discussed further, its presence can be probably connected with multiple coordination shells crossings in that region. One can easily see that the plot is symmetric around the line of $u = 0.25$.

The total energy profiles in the $(c/a,u)$ plane calculated for Bi at the equilibrium volume of the A7 structure within

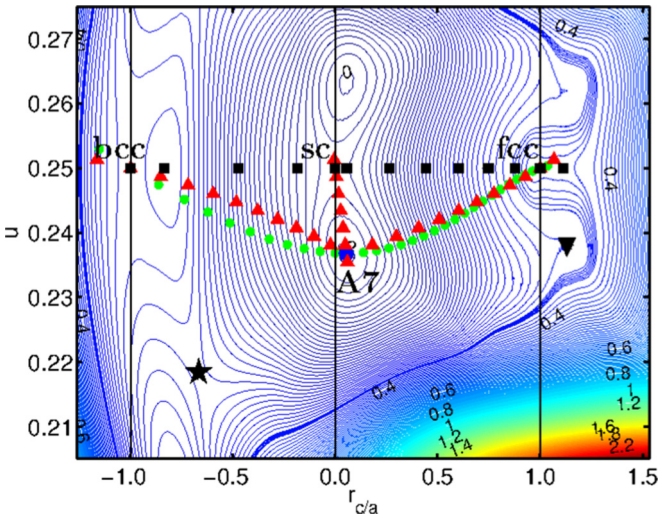


FIG. 4. The behavior of the total energy of Sb in the $(c/a,u)$ plane, calculated within the LDA at the equilibrium atomic volume of the A7 structure, $V/V_{\mathrm{exp}} = 0.977$. Total energies of cubic structures correspond to stationary points and they are indicated by black squares lying at the vertical black lines. The fourth stationary point, the A7 structure, is indicated by single large blue dot. The saddle point close to the bcc region is marked by a star, a secondary minimum close to the fcc region is marked by a downward pointing triangle. (Let us note that this minimum is not fully evolved as, e.g., in the case shown in Fig. 24 from Appendix C). The deformation paths studied are indicated by curves shown by black squares (trigonal deformation path bcc-sc-fcc with $u = 0.25$, further also BSF-lin path) and red triangles [two linear segments $u(c/a)$ bcc-A7 and A7-fcc used to create the BAF-lin path and one linear segment $u(c/a)$ A7-sc (AS-lin)]. Green circles show a cubic function $u(c/a)$ connecting the bcc, A7, and fcc structures (BAF-cub).

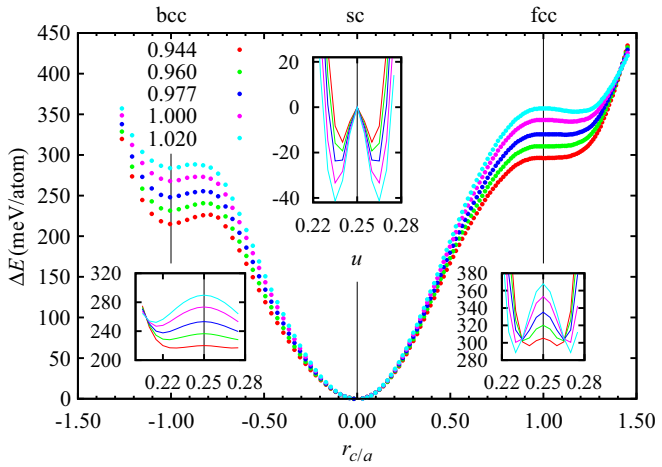


FIG. 5. Total energy profiles of Sb along the trigonal deformation path (BSF-lin) calculated within the LDA at various fixed volumes $V/V_{\mathrm{exp}}$ (given in the upper left corner together with the corresponding colors). The insets show the behavior of $E(u)$ in the neighborhood of the cubic structures ($u = 0.25$). The total energy is set to zero at the sc structure for all volumes considered. The units along the vertical axis are the same both in the main plot and the insets. The description of the vertical axis in the insets is omitted.

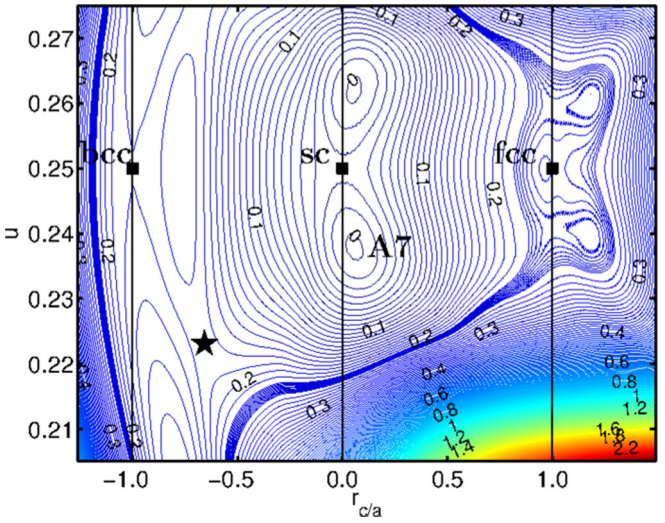


FIG. 6. Total energy profile $E(c/a,u)$ (eV/at) of Bi calculated within the LDA at the equilibrium volume of the A7 structure $V/V_{\text{exp}} = 0.958$. Total energy minimum for the A7 structure is shifted to zero.

the LDA and LDA+SOC are displayed in Figs. 6 and 7; they are very similar to Fig. 4 obtained for Sb. The equilibrium A7 structure corresponds to the absolute minimum of the total energy. Two of the basic cubic structures, bcc, and sc, exhibit a saddle point—these are symmetry-dictated stationary points. The fcc structure can exhibit a local maximum or minimum of total energy with respect to $u$ depending on atomic volume (Fig. 8).

Figure 8 for Bi is analogous to Fig. 5. Here we can see again that for bcc and sc structures the total energy exhibits a minimum with respect to $r_{c/a}$ and a maximum with respect to $u$, so that in two-dimensional plot for a fixed volume (as in Fig. 7), we would have saddle points for these structures, although the saddle point for bcc structure at $V/V_{\text{exp}} = 0.958$

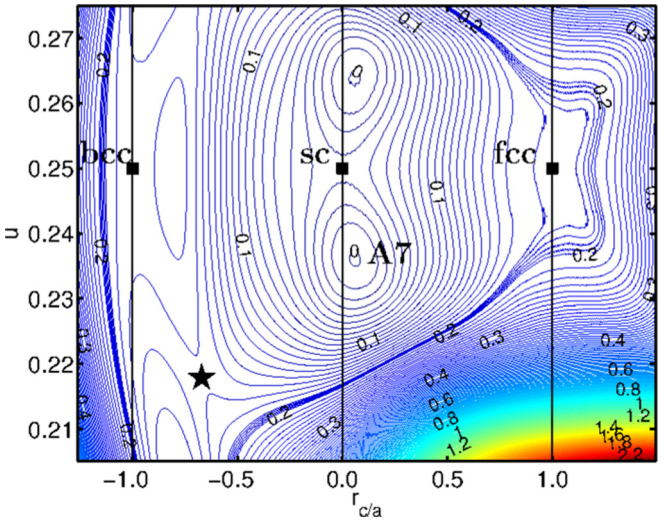


FIG. 7. Total energy profile $E(c/a,u)$ (eV/at) of Bi calculated within the LDA+SOC approach at the equilibrium volume of the A7 structure $V/V_{\text{exp}} = 0.987$. Total energy minimum for the A7 structure is shifted to zero.

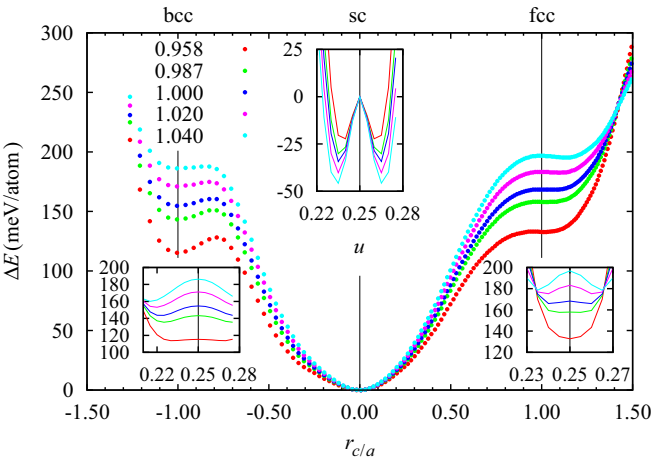


FIG. 8. Total energy profiles of Bi along the trigonal deformation path (BSF-lin) calculated within the LDA+SOC at various fixed volumes $V/V_{\text{exp}}$ (given in the upper left corner together with the corresponding colors). The insets show the behavior of $E(u)$ in the neighborhood of the cubic structures ($u = 0.25$). The total energy is set to zero at the sc structure for all volumes considered. The units along the vertical axis are the same both in the main plot and the insets. The description of the vertical axis in the insets is omitted.

would be very flat with respect to $u$, and at $V/V_{\text{exp}} = 1.040$, we would have nearly an inflexion point with respect to $r_{c/a}$. On the other hand, for fcc structure, the total energy exhibits an inflexion point with essentially zero derivative with respect to $r_{c/a}$ almost for all volumes studied, whereas, with respect to $u$, we encounter a minimum for lower volumes and a maximum for higher volumes.

With increasing volume, the position of the lowest-energy (at that volume) A7 structure changes slightly—the $c/a$ increases, in order to keep up with the increasing volume, and $u$ moves more away from the 0.25, which is the value corresponding to the trigonally deformed cubic structures (see Table IV). The change of $u$ can be explained as follows: when we decrease the volume, i.e., we apply some pressure, all three elements should transform to bcc structure (with some intermediate steps). This means that the internal parameter $u$ should approach the value of 0.25. Of course, our deformation paths are too simple to account for the observed complex intermediate structures but this volume trend of $u$ of the volume-deformed A7 structure agrees nicely with the experimental observations that reveal approaching to a cubic structure.

The presence of the saddle point near the bcc structure (denoted by a star in Figs. 4, 6, and 7) is preserved in all three elements and at various volumes indicating that this is probably a geometrical (structural) effect. The character of changes of its position with increasing volume is very similar as in case of the lowest-energy A7 structure, i.e., $c/a$ increases but $u$ decreases. Table IV demonstrates this general fact in case of Bi. The dependence of corresponding $c/a$ and $u$ on volume is nearly linear. The coordinates of the saddle point corresponding to the A7 structure at several atomic volumes may be found in the upper part of Table IV for Bi and in Table IX in Appendix B for As and Sb. Figure 23 in this Appendix shows then the total energy profile for Bi calculated within the LDA+SOC approach.

TABLE IV. Coordinates of selected points in the $(c/a,u)$ plane as functions of atomic volume in case of Bi, obtained from the LDA and LDA+SOC calculations.

| Saddle point A7 structure | LDA | | | LDA+SOC | | |
|---|---|---|---|---|---|---|
| $V/V_{\rm exp}$ | $r_{c/a}$ | $c/a$ | $u$ | $r_{c/a}$ | $c/a$ | $u$ |
| 0.958 | −0.67 | 1.54 | 0.223 | ≈−0.72 | ≈1.48 | ≈0.226 |
| 0.987 | −0.64 | 1.57 | 0.219 | −0.67 | 1.54 | 0.218 |
| 1.000 | −0.63 | 1.59 | 0.218 | −0.65 | 1.57 | 0.215 |
| 1.020 | −0.61 | 1.61 | 0.216 | −0.61 | 1.60 | 0.212 |
| 1.040 | −0.59 | 1.63 | 0.214 | −0.58 | 1.64 | 0.209 |
| Lowest-energy A7 structure | | LDA | | | LDA+SOC | |
| 0.958 | 0.06 | 2.55 | 0.238 | 0.05 | 2.54 | 0.237 |
| 0.987 | 0.07 | 2.57 | 0.236 | 0.06 | 2.56 | 0.236 |
| 1.000 | 0.09 | 2.60 | 0.236 | 0.07 | 2.57 | 0.235 |
| 1.020 | 0.10 | 2.62 | 0.234 | 0.07 | 2.57 | 0.235 |
| 1.040 | 0.12 | 2.66 | 0.233 | 0.09 | 2.60 | 0.233 |
| A7 structure at lobes | | LDA | | | LDA+SOC | |
| 0.958 | 1.17 | 5.53 | 0.240 | | | |
| 0.987 | 1.22 | 5.70 | 0.237 | | | |
| 1.000 | 1.24 | 5.79 | 0.236 | 1.15 | 5.43 | 0.241 |
| 1.020 | 1.28 | 5.94 | 0.233 | 1.18 | 5.57 | 0.238 |
| 1.040 | 1.30 | 6.03 | 0.232 | 1.23 | 5.73 | 0.236 |

We may expect that the presence of this saddle point may be related to multiple coordination shell crossings in the corresponding crystal structure. A similar hypothesis has already been suggested in a study of (fixed volume) trigonal deformation paths in Fe, Co, and Ni (see Ref. [40]). Those authors have found that the trigonal deformation path contains—apart from the bcc, sc, and fcc structures—another two structures that influence the behavior of total energy differences between various magnetic modifications. The corresponding values of $c/a$ in the original "1-2-4" notation were 1.27 and 2.83 (the exact values are $\sqrt{8/5}$ and $\sqrt{8}$), which corresponds, respectively, to $r_{c/a}$ (and $c/a$) values of −0.66 (1.55) and 0.50 (3.46) in our notation. The radii of the coordination shells in some A7 structures corresponding to the saddle point given in Table IV are displayed in Figs. 9–11.

Figure 9 shows the radii of coordination shells as functions of $r_{c/a}$ at $V/V_{\rm exp}=1$ and $u=0.215$ belonging to the saddle point in Bi, Fig. 10 corresponds to $u=0.25$, and Fig. 11 exhibits the dependence of the selected coordination shell radii on the parameter $u$ at fixed $c/a=1.57$. We may observe a degeneracy and more crossings in the cases of cubic structures or their trigonally deformed variants, although the general A7 structures and the structures on trigonal deformation path (except for bcc, sc, and fcc structures) have the same space group. The degeneracy of coordination shell radii in case of $u=0.25$ can be very well understood if we compare the distances between the atom at the trigonal axis in atomic plane B and its neighbors in atomic planes c (below B) and a (above B) in Figs. 1 and 2. In case of a general A7 structure (Fig. 1, $u\neq 0.25$) they do differ, but they coincide in

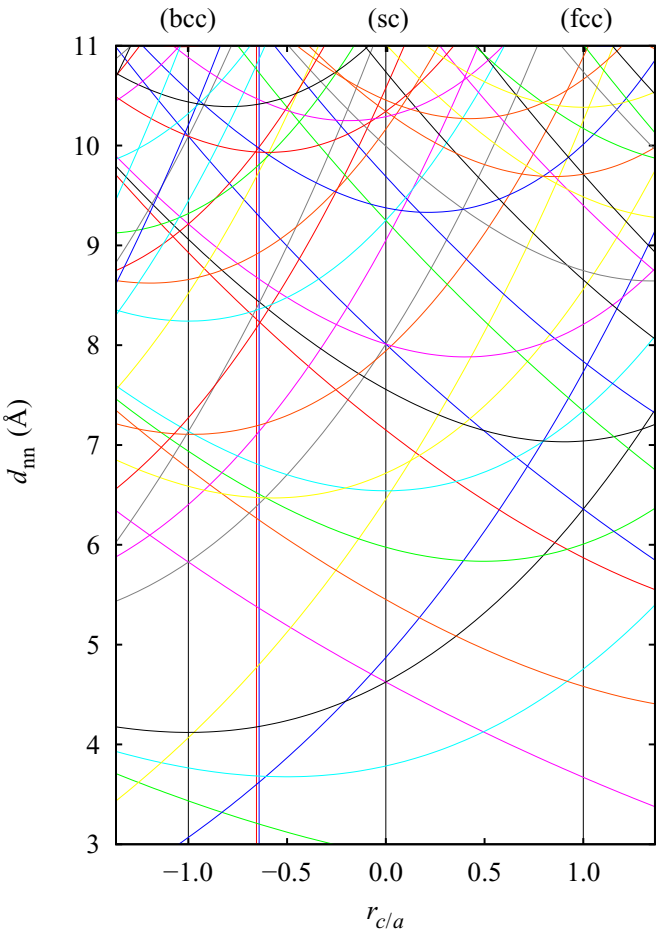


FIG. 9. Radii of coordination shells of the A7 structures displayed as functions of $r_{c/a}$ for a fixed $u=0.215$ (corresponding to position of saddle point in case of Bi, calculated within the LDA+SOC approach at $V/V_{\rm exp}=1$). The vertical lines ordered from left to right show the $r_{c/a}$ of the bcc structure (black), of the "at $c/a=1.27$" structure of Ref [40] (red), of the saddle point structure (blue) with $c/a=1.57$ (1.28 in the "1-2-4" notation), and of the sc (black) and fcc structures (black). As $u\neq 0.25$, the black lines correspond to A7 structures at $u=0.215$ which are closest to bcc, sc and fcc structures; therefore, these structures are shown in parentheses in this figure. Let us note that the radius of the coordination shell represented by a green curve in the lower left corner of this figure attains a minimum at $r_{c/a}\approx 0.8$ and increases again for higher values of $r_{c/a}$; no intersections have been found for $d_{nn}<3$ Å.

the structures lying on the trigonal deformation path (Fig. 2, $u=0.25$), independently on the value of $c/a$. Thus, some coordination shells split if we change $u$ from 0.25 to some other value. This also follows from Eq. (2).

The structure at $c/a\doteq 1.27$ (in the "1-2-4" notation) and with $u=0.25$ found in the Ref. [40] exhibits a lot of intersections that lie precisely above each other. In case of the A7 structure with $u\doteq 0.215$, the degeneracy is partially removed, but the crossings are not strictly localized at one value of $c/a$. Figure 9 displaying range of the coordination shell radii between 3 and 11 Å shows that there are approximately 20 double and one triple crossings within range $c/a\in[1.50,1.65]$ (corresponding approximately

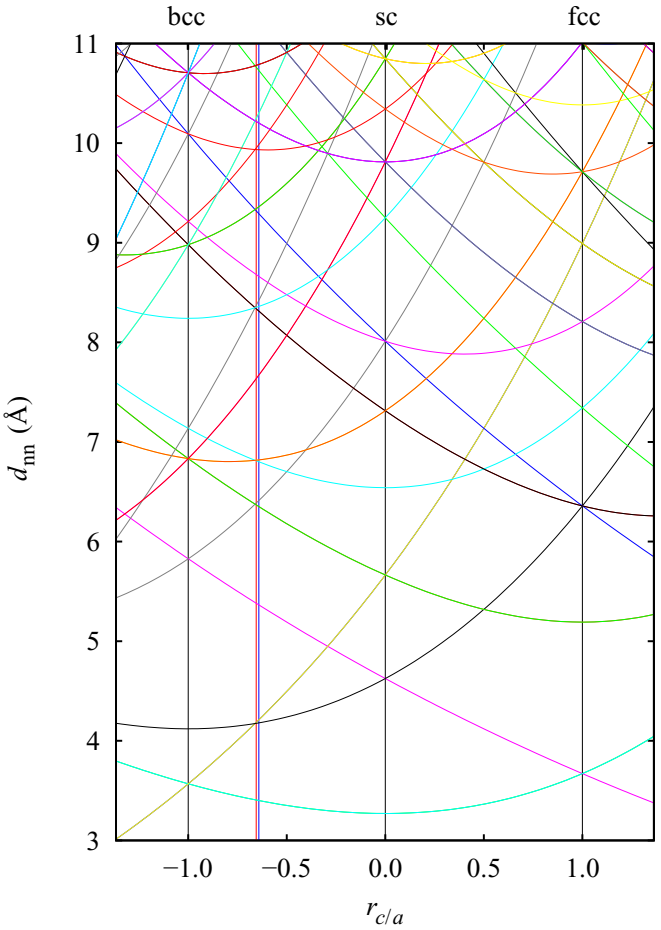


FIG. 10. The same as Fig. 9 but for $u = 0.25$ corresponding to the trigonally deformed cubic structures. Let us note that some of the shells from the previous figure coincide and there are more crossings at the $c/a$ values corresponding to the three cubic structures.

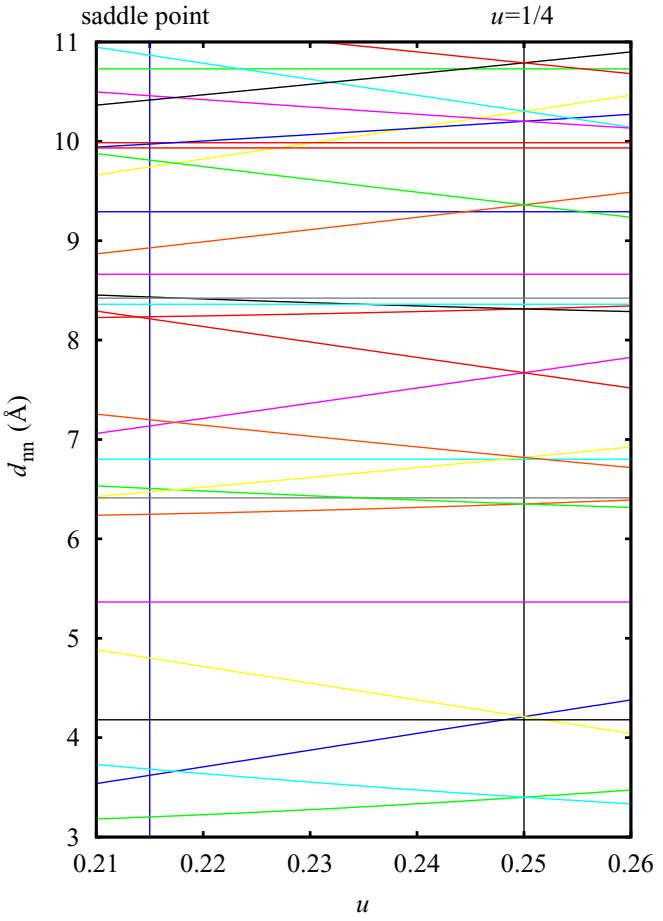


FIG. 11. Analogue of Fig. 9 but radii are displayed as functions of $u$ for a fixed $c/a = 1.57$ (corresponding to position of saddle point in case of Bi, LDA+SOC, $V/V_{exp} = 1$). We have indicated two values of $u$ by vertical lines—the saddle point (blue, left, $u = 0.215$) and $u = 1/4$ corresponding to a trigonally distorted cubic structures (black, right).

to $r_{c/a} \in [-0.71, -0.57]$) belonging to the A7 structure at the saddle point in Bi calculated within the LDA+SOC at $V/V_{exp} = 1$ and $c/a \doteq 1.57$. From Fig. 11, we may see that in the neighborhood of $u = 0.215$ corresponding to the saddle point structure many coordination shells coincide as well. Thus we may conclude that the observed saddle point in total energy profiles corresponds to the location of coordination shell crossings.

We have not found any stationary point in the total energy profile corresponding to the saddle point near fcc from Ref. [40] ($c/a = \sqrt{8} \doteq 2.83$ in the notation of Ref. [40]; this corresponds to $c/a \doteq 3.47$ and $r_{c/a} = 0.5$ in our notation). The coordination shells displayed in Fig. 10 have a crossing close to the corresponding value of $c/a$ but the calculated total energy $E(c/a,u)$ plots (shown for Bi in Figs. 6 and 7 and for Sb in Fig. 4) exhibit no special points there. But the one-dimensional energy profiles along trigonal deformation path displayed in Figs. 5 (Sb) and 8 (Bi) exhibit inflexion points in that region (at $r_{c/a} = 0.45$–$0.46$ and $r_{c/a} = 0.49$–$0.50$, the range of $r_{c/a}$ is due to a slight dependence of the position of the inflexion point on atomic volume).

The "lobe" structure, marked by a downward pointed triangle in Fig. 4, is developed to a different degree in different materials, as it may be seen from comparison of the total energy profile of Sb calculated using the LDA (Fig. 4) with those of Bi obtained within the LDA and LDA+SOC (Figs. 24 and 25 in Appendix C). A more detailed analysis of the total energy contour plots at various volumes (presented in Appendix C) reveals that the lobe structure is usually more pronounced at higher atomic volumes.

To summarize this section, we have found some other stationary points, not corresponding to the equilibrium A7, bcc, sc, and fcc structures. Positions of these stationary points, not determined by symmetry, depend on volume and their presence or absence is the property of the particular element.

### C. Deformation at variable volume

Figure 12 shows the contour plot of total energy of Bi along the trigonal deformation path with the cubic structures located along the path in accordance with Table II; their atomic volumes are given in Table III. The total energy was calculated within the LDA+SOC approach.

We see that both bcc and sc structures in Bi correspond to total energy minima, and it is also the case for the calculations

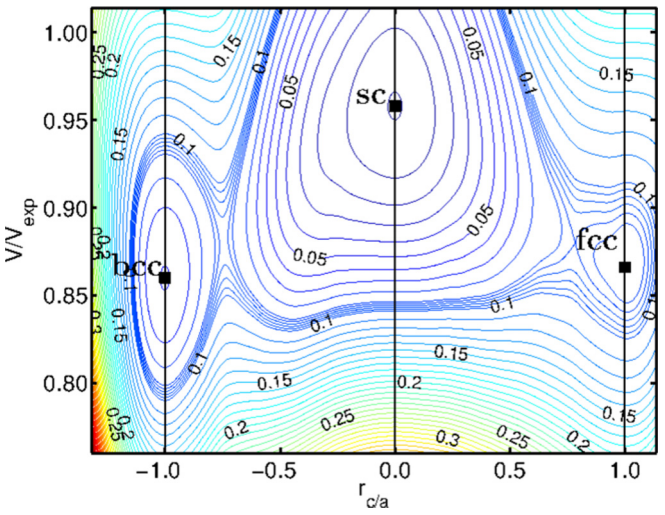


FIG. 12. Total energy profile $E(c/a,V)$ (eV/at) of Bi calculated within the LDA+SOC approach along the BSF-lin path. Total energy minimum corresponding to the sc structure is shifted to zero. Let us note that the saddle points at $r_{c/a}$ equal approximately $-0.75$ and 0.77 do not correspond to the two structures discussed in Ref. [40].

performed within the LDA, GGA, and GGA+SOC. This is slightly different when compared to the results for Po, ground state of which is the sc structure. As we can see from Figs. 18–20 of Ref. [34], in Po the sc structure also corresponds to the total energy minimum, but the bcc structure exhibits either a local symmetry-dictated minimum (Fig. 20 of Ref. [34], LDA+SOC calculation) or a symmetry-dictated saddle point accompanied by a very near local minimum not dictated by symmetry at slightly lower values of $c/a$ (Figs. 18 and 19 of Ref. [34], GGA and LDA calculations).

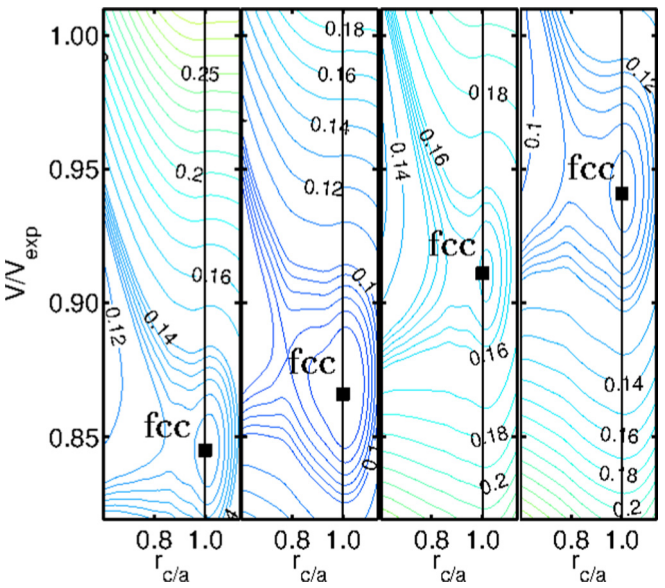


FIG. 13. Details of total energy profiles $E(c/a,V)$ (eV/at) of Bi along the BSF-lin path calculated within the LDA, LDA+SOC, GGA, and GGA+SOC approach (from left to right). The total energy minimum of the sc structure is shifted to zero in each segment. Vertical axis is the same for all segments of the plot and its description is given in the leftmost segment.

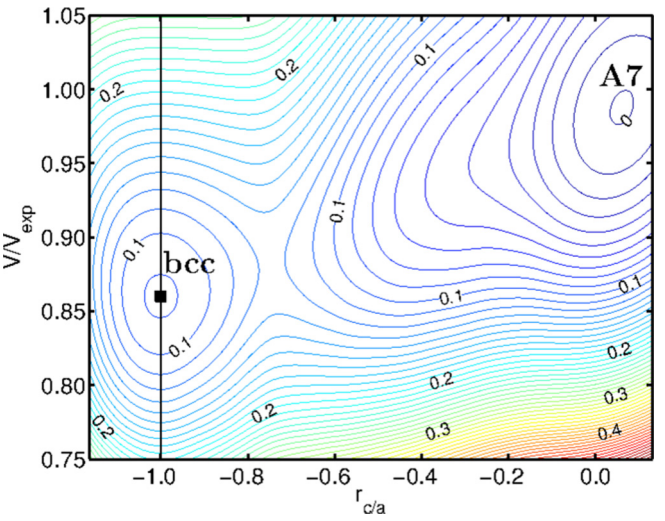


FIG. 14. Total energy profile $E(c/a,V)$ (eV/at) of Bi calculated within the LDA+SOC approach along the BAF-lin path from the bcc to A7 structure. Total energy minimum of the lowest-energy A7 structure is shifted to zero.

Figure 13 presents variations of equilibrium volume of the fcc structure of Bi due to changing the approximation of the exchange-correlation energy. We can see that the equilibrium volume increases from LDA, through LDA+SOC, GGA to GGA+SOC. Here the fcc structure exhibits either a symmetry-dictated local minimum or a saddle point accompanied by a very near local minimum not dictated by symmetry at slightly higher values of $c/a$. On the other hand, the fcc structure in Po corresponds either to a symmetry-dictated minimum (Fig. 19 of Ref. [34], LDA calculation) or to a saddle point accompanied by a relatively far local minimum not dictated by symmetry at considerably higher values of $c/a$ (Figs. 18 and 20 of Ref. [34], GGA and LDA+SOC calculations). Generally, the atomic volumes of both bcc and fcc structures are lower than the atomic volume of sc structure in case of all elements discussed, i.e., As, Sb, Bi, and Po. The difference between

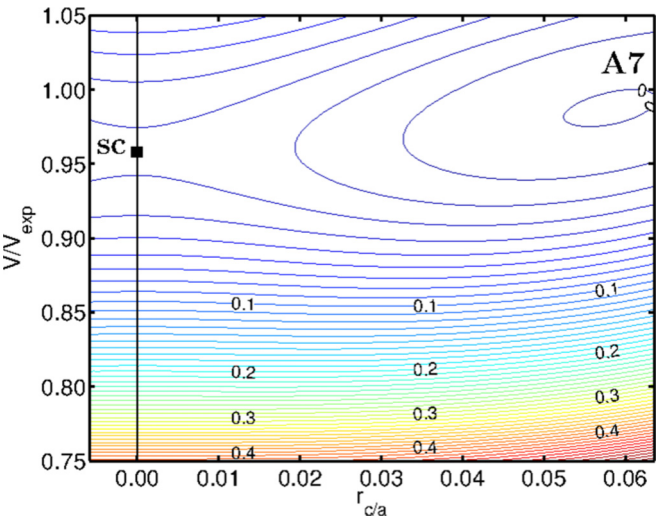


FIG. 15. The same as 14 but along the AS-lin path (from sc to A7 structure).

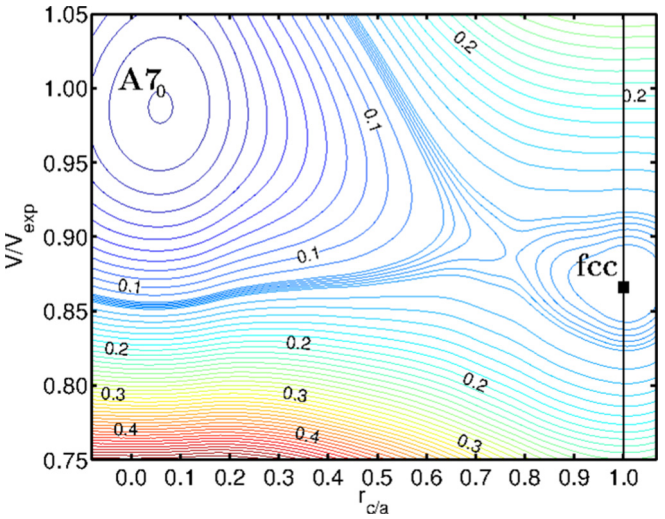


FIG. 16. The same as 14 but along the BAF-lin path from A7 to fcc structure.

the sc and bcc or fcc atomic volumes in Po is about 10% of experimental atomic volume for all three approximations of the exchange-correlation energy examined in Ref. [34]. Similar values were obtained for the heavier elements Sb and Bi in this work (see Table III), but the volume difference in case of As is approximately half of that value.

Figures 14–16 show the behavior of total energy of Bi calculated within the LDA+SOC along the linear segments connecting A7 and the bcc, fcc, and sc structures (cf. Fig. 4). Let us note that total energy profiles displayed in Figs. 14 and 16 corresponding to the BAF-lin path are very similar to corresponding portions of the total energy profile along the BAF-cub path displayed in Fig. 17.

Now, let us consider the profile of total energy of Bi along the linear segment sc-A7 in the $(c/a,u)$ plane displayed in Fig. 15. One can see that sc structure corresponds to a saddle point now, i.e., it changes its type from a minimum to a saddle

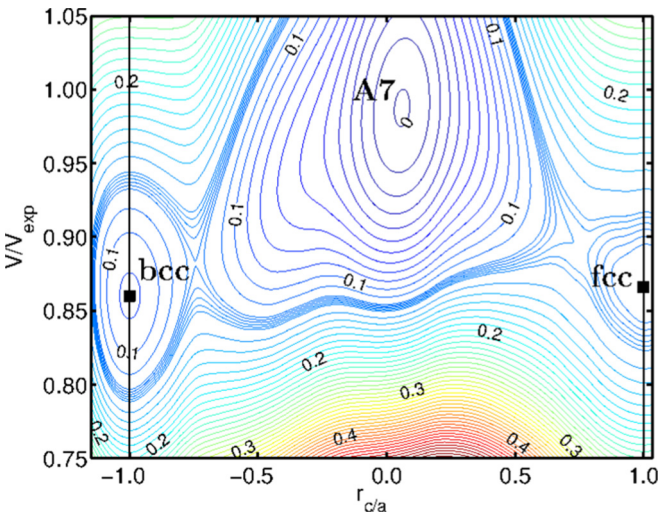


FIG. 17. Total energy profile $E(c/a,V)$ (eV/at) of Bi calculated within the LDA+SOC approach along the BAF-cub path. Total energy minimum of the lowest-energy A7 structure is shifted to zero.

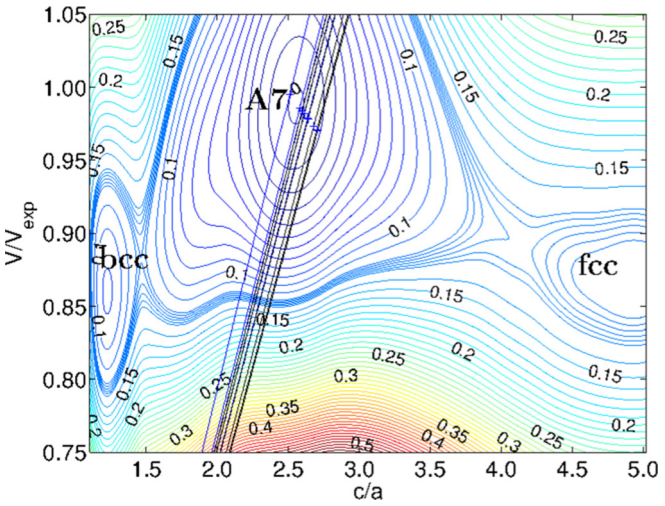


FIG. 18. Total energy profile $E(c/a,V)$ (eV/at) of Bi calculated within the LDA+SOC approach along the BAF-cub path. Total energy minimum of the lowest-energy A7 structure is shifted to zero. The straight lines correspond (from left to right) to the substrates Al(111), Ba(111), Co(0001), Si(111) (Ref. [51]), Pb(111), Si(111) (Ref. [7]), Rh(111), Si(111) (Ref. [8]), Si(111) (Ref. [12]), Ge(111) (Ref. [13]), Si(111) (Ref. [11]), and Si(111) (Ref. [9]). The black straight lines in the plot correspond to experimental data (Table V), the blue lines represent the cases given in Table VI selected for our predictions. Energy minima along all of the straight lines are denoted by blue crosses. As the straight lines are very close together, we give a more detailed representation of the comparison of our results with experiment and our theoretical predictions in Figs. 21 and 22.

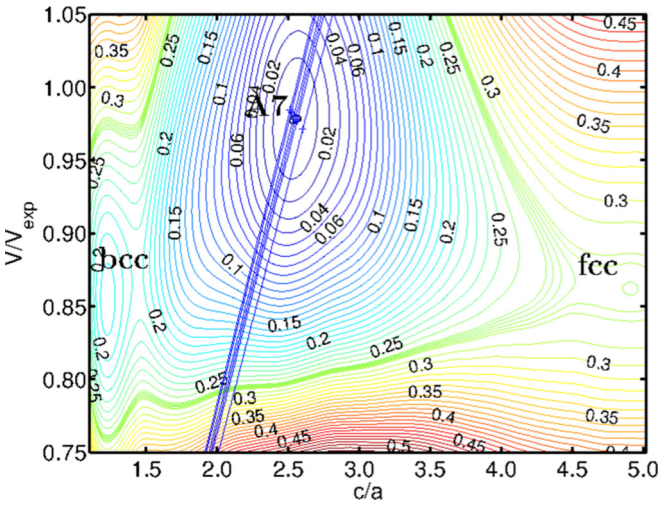


FIG. 19. The same as in Fig. 18 but for Sb instead of Bi. The straight lines correspond (from left to right) to the substrates Ag(111), Au(111), C(0001), Rh(111), Al(111), and Zn(0001). The blue crosses represent the predicted configurations of the Sb films on these substrates; the corresponding numerical values of the structural parameters $c/a$ and $u$ are given in Table VI. As the straight lines are very close together, we give a more detailed representation of our theoretical predictions in Fig. 22.

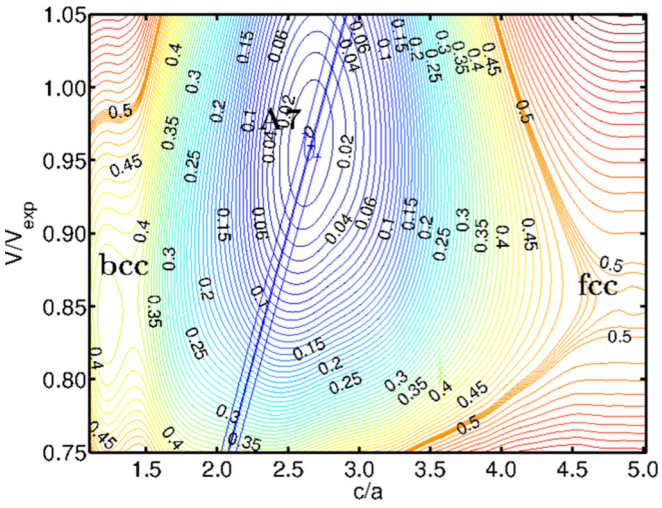


FIG. 20. The same as in Fig. 18 but for As instead of Bi. The straight lines correspond (from left to right) to the substrates Ti(0001), Rh(111), Co(0001), and Zn(0001). The blue crosses represent the predicted configurations of the As films on these substrates; the corresponding numerical values of the structural parameters $c/a$ and $u$ are given in Table VI. As the straight lines are very close together, we give a more detailed representation of our theoretical predictions in Fig. 22.

point when compared to BSF-lin path (Fig. 12). This change could have been anticipated as sc structure corresponds to a saddle point in the $(c/a,u)$ plane (Figs. 7–8).

The main difference between the total energy profiles along the BAF-lin path (see the separated segments in Figs. 14 and 16) and BSF-lin path (Fig. 12) is that the minimum in the BSF-lin plot at $r_{c/a} = 0$ corresponding to the sc structure is shifted to the minimum in the BAF-lin plot at $r_{c/a} \approx 0.1$ corresponding to the A7 structure. The contour plots BAF-lin and BAF-cub are almost identical, hence, for the sake of brevity, we omit the figures related to the former path.

### D. Contour plots applied to epitaxial thin films: Methodology and comparison with experiment

A hexagonal (0001)-oriented A7 structure-based thin films can be described by the values of the in-plane lattice parameter $a$, bilayer-bilayer step height $c/3$ and internal parameter $u$. Our method to determine the $c/3$ and also $u$ from the total energy $E$ contour plots for a given in-plane lattice parameter $a$ (determined usually by the substrate) is as follows. Since we consider the direction [0001] perpendicular to the substrate plane, the volume per atom can be easily related to $c/a$ as

$$\frac{V(c/a)}{V_{\rm exp}} = \frac{a^2 c}{a_{\rm exp}^2 c_{\rm exp}} = \frac{a^3}{a_{\rm exp}^2 c_{\rm exp}}\, c/a = k(a)\, c/a, \qquad (5)$$

where $k(a)$ determines the slope of the linear relation between the atomic volume and $c/a$.

To get the total energy minimum corresponding to a thin film of As, Sb or Bi on a particular (111) or (0001) substrate, we may use the BAF-cub LDA+SOC contour plots shown in Figs. 18–20. They allow us to determine the $c/a$ for thin films of these elements once the $a$ is given. Here $r_{c/a}$ is used as the variable along the horizontal axis which ensures that a straight line corresponds to a given substrate represented by a certain value of the in-plane lattice constant $a$.

It is sufficient to draw the lines $V/V_{\rm exp} = k(a) \times (c/a)$, with $k(a)$ determined using the Equation (5), so that the $c/a$ ratio for a given $a$ is

$$\frac{c}{a} = \frac{1}{k(a)}\frac{V}{V_{\rm exp}} = \left(k' \frac{V_{\rm exp}}{a^3}\right)\left(\frac{V}{V_{\rm exp}}\right),\ k' = 4\sqrt{3}. \qquad (6)$$

This is a simple re-arrangement of Eq. (5) better suited to the methodology of determination of structural parameters. These lines are displayed in contour plots in Figs. 18–20. Experimental values of atomic volumes are given in Table I.

To determine quickly the values of $c/a$ at the lower and upper boundaries of Figs. 18–20, i.e., for the values of $V/V_{\rm exp} = 0.75$ and 1.05, for any substrate with the in-plane lattice constant $a$, coefficients presented in Table VII may be used. For example, let us consider a substrate with $a = 4.581$ Å (representing the Al(111) surface). The value of $c/a$ corresponding to the straight line for this substrate at $V/V_{\rm exp} = 0.75$, i.e., at the bottom of contour plot for Bi in Fig. 18, is given by $c/a(0.75) \doteq 181.8/(a[\text{Å}])^3 \doteq 1.891$, and for $V/V_{\rm exp} = 1.05$ we obtain $c/a(1.05) \doteq 254.5/(a[\text{Å}])^3 \doteq 2.647$, as it may be seen in Fig. 18 (the leftmost substrate straight line).

Now, the equilibrium configuration of the As, Sb, or Bi film on a particular substrate corresponds to the energy minimum along the straight line for this substrate in the relevant contour plot in Figs. 18, 19, or 20. This minimum determines the $c/a$, and, consequently, also $u$ from the $u = u(c/a)$ dependence of a selected plot. The values of structural parameters corresponding to this minimum are assumed to be those of the film. As the straight lines for various substrates are very close to each other, we present the details of the plots in Figs. 21 and 22.

In this section, let us discuss the comparison of our calculated values with available experimental results for Bi thin films (we were not able to find any experiment delivering the data for the As and Sb thin films). Table V shows these parameters determined for Bi thin films grown mostly on a Si substrate. The second and third column contain experimental values of $a$ and $c/3$, respectively, the remaining columns exhibit the values of structural parameters $c/3$, $c/a$, $V/V_{\rm exp}$, and $u$ determined with the help of total energy contour plots calculated along the BAF-lin and BAF-cub paths within the LDA+SOC approach (see Fig. 18 and more detailed Fig. 21 for the BAF-cub contour plots). Our values of $c/3$ obtained using the BAF-cub path are in a very good agreement with the experimental values in most cases. The data on Bi/Si films from Refs. [7] and [12] and Bi/Ge films from Ref. [13] have a large error range, and although our theoretical results do not necessarily match the mean value of $c/3$ in the best way, they are very well within the error range and not very far from the mean value. As no experimental paper has given the value of $u$ for the film, our values of $u$ presented in Table V may be considered as theoretical predictions.

We can see that there is a little effect of the path we have chosen to connect bcc, A7, and fcc structures in the plane $(c/a,u)$. Since the larger BAF-cub values agree better with the experimental ones, we may speculate that the BAF-cub path is closer to minimum energy path connecting the three structures

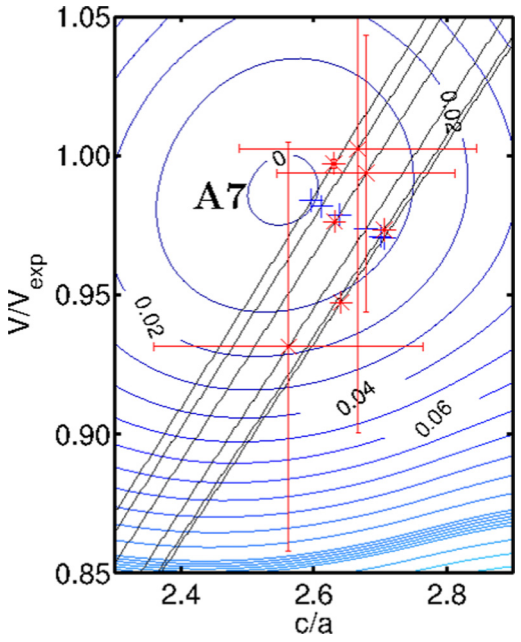


FIG. 21. Detailed comparison of our results with experimental data from Table V. This figure is an enlarged part of Fig. 18 with the theoretical predictions left out. The experimental points are denoted by red stars with error bars whenever available, our calculated results are marked by blue crosses. The straight lines correspond (from left to right) to the substrates Si(111) (Ref. [51]), Si(111) (Ref. [7]), Si(111) (Ref. [8]), Si(111) (Ref. [12]), Ge(111) (Ref. [13]), Si(111) (Ref. [11]), and Si(111) (Ref. [9]).

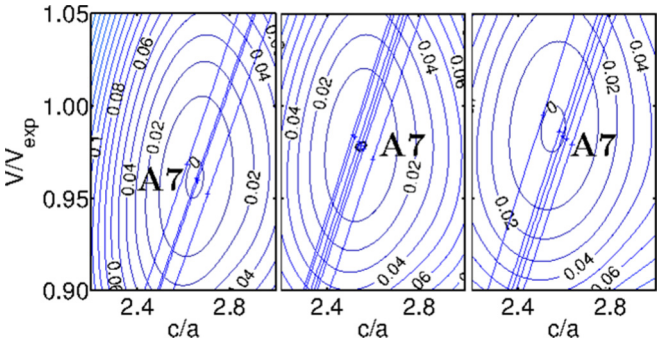


FIG. 22. The predicted configurations of As, Sb, and Bi (from left to right) thin films on selected substrates. The figures represent details of the neighborhood of the A7 structure from Figs. 20, 19, and 18, respectively. The straight lines correspond (from left to right) to the substrates: Ti(0001), Rh(111), Co(0001), and Zn(0001) in case of As; Ag(111), Au(111), C(0001), Rh(111), Al(111), and Zn(0001) in case of Sb; Al(111), Ba(111), Co(0001), Pb(111), and Rh(111) in case of Bi. The predicted configurations are marked by crosses and the corresponding numerical values of the structural parameters $c/a$ and $u$ are given in Table VI. Vertical axis is the same for all segments of the plot and its description is given in the leftmost segment.

than the BAF-lin path, at least in the neighborhood of the A7 structure. This is also confirmed by the results of our bulk test discussed in the Appendix D. Thus the BAF-cub contour plot calculated within the LDA+SOC approach may be regarded as the best match to the experimental thin film data.

TABLE V. Structural parameters of thin Bi(0001) films [mostly on Si(111) but also on Ge(111) substrates] obtained from total energy contour plots along the BAF-lin and BAF-cub paths calculated within the LDA+SOC approach. In some cases, we give three values of $c/3$ obtained from our plots which correspond to lower bound, mean value and upper bound of the experimental range of the parameter $a$.

| | Experiment | | Present calculations | | | | |
|---|---|---|---|---|---|---|---|
| Subs. | $a$ (Å) | $c/3$ (Å) | path | $c/3$ (Å) | $c/a$ | $V/V_{\text{exp}}$ | $u$ |
| Si[a] | $(4.5 \pm 0.2)$ | $(4.0 \pm 0.2)$ | BAF-lin | 4.16-3.90-3.73 | 2.60 | 0.977 | 0.238 |
| | | | BAF-cub | 4.17-3.92-3.75 | 2.61 | 0.982 | 0.238 |
| Si[b] | 4.48 | ≈3.93 | BAF-lin | 3.92 | 2.63 | 0.974 | 0.238 |
| | | | BAF-cub | 3.94 | 2.64 | 0.979 | 0.238 |
| Si[c] | 4.43 | ≈3.9 | BAF-lin | 3.98 | 2.70 | 0.967 | 0.239 |
| | | | BAF-cub | 4.00 | 2.71 | 0.972 | 0.239 |
| Si[d] | 4.434 | ≈4 | BAF-lin | 3.98 | 2.69 | 0.968 | 0.239 |
| | | | BAF-cub | 3.99 | 2.70 | 0.971 | 0.239 |
| Si[e] | $(4.480 \pm 0.004)$ | $(4.0 \pm 0.2)$ | BAF-lin | 3.93-3.92-3.92 | 2.63 | 0.974 | 0.238 |
| | | | BAF-cub | 3.94-3.94-3.94 | 2.64 | 0.979 | 0.238 |
| Ge[f] | 4.45 | $(3.8 \pm 0.3)$ | BAF-lin | 3.96 | 2.67 | 0.970 | 0.239 |
| | | | BAF-cub | 3.97 | 2.68 | 0.973 | 0.239 |
| Si[g] | $(4.512 \pm 0.002)$ | $(3.957 \pm 0.005)$ | BAF-lin | 3.89-3.89-3.89 | 2.59 | 0.980 | 0.238 |
| | | | BAF-cub | 3.91-3.91-3.90 | 2.60 | 0.985 | 0.238 |

[a]Reference [7].
[b]Reference [8].
[c]Reference [9].
[d]Reference [11].
[e]Reference [12].
[f]Reference [13].
[g]Reference [51].

TABLE VI. Predicted values of structural parameters $c/3$ and $u$ for As, Sb, and Bi thin films with the A7 structure on selected substrates determined with the help of total energy contour plots along the BAF-cub path calculated within the LDA+SOC approach. The mismatch $\Delta a/a$ is defined as $\Delta a/a = (a_{\text{film}}/a_{\text{bulk}} - 1) \times 100\%$.

| Element | Substrate | Magic $\frac{a_{\text{sub}}}{a_{\text{film}}}$ | Assumed $a$ (Å) | Assumed $\frac{\Delta a}{a}$ (%) | Predicted structural parameters $c/3$ (Å) | $c/a$ | $V/V_{\text{exp}}$ | $u$ |
|---|---|---|---|---|---|---|---|---|
| As | Ti(0001) | 7/9 | 3.794 | −0.9 | 3.31 | 2.62 | 0.97 | 0.233 |
| | Rh(111) | 5/7 | 3.765 | −0.1 | 3.33 | 2.66 | 0.96 | 0.233 |
| | Co(0001) | 2/3 | 3.761 | −0.03 | 3.34 | 2.66 | 0.96 | 0.233 |
| | Zn(0001) | 5/7 | 3.731 | 0.8 | 3.37 | 2.71 | 0.95 | 0.234 |
| Sb | Ag(111) | 2/3 | 4.333 | −0.8 | 3.63 | 2.51 | 0.98 | 0.238 |
| | Au(111) | 2/3 | 4.326 | −0.6 | 3.64 | 2.52 | 0.98 | 0.238 |
| | C(0001) | 4/7 | 4.312 | −0.3 | 3.65 | 2.54 | 0.98 | 0.238 |
| | Rh(111) | 5/8 | 4.303 | −0.1 | 3.66 | 2.55 | 0.98 | 0.238 |
| | Al(111) | 2/3 | 4.295 | 0.1 | 3.67 | 2.56 | 0.98 | 0.238 |
| | Zn(0001) | 5/8 | 4.264 | 0.9 | 3.70 | 2.60 | 0.97 | 0.239 |
| Bi | Al(111) | 5/8 | 4.581 | −1.1 | 3.83 | 2.51 | 1.00 | 0.238 |
| | Ba(111) | 11/7 | 4.525 | 0.2 | 3.89 | 2.58 | 0.99 | 0.238 |
| | Co(0001) | 5/9 | 4.513 | 0.4 | 3.90 | 2.60 | 0.98 | 0.238 |
| | Pb(111) | 7/9 | 4.501 | 0.7 | 3.92 | 2.61 | 0.98 | 0.238 |
| | Rh(111) | 3/5 | 4.482 | 1.1 | 3.94 | 2.64 | 0.98 | 0.238 |

### E. Epitaxial thin film application: predictions

In epitaxially grown thin films of Fe, Co, and Ni, the lattice parameter $a$ of the film in the plane of the substrate is fully determined by the substrate (a more detailed analysis may be found, e.g., in Refs. [30–32,40]). Unfortunately, for As, Sb, and Bi films, there is no simple and unique way to determine this lattice parameter from that of the substrate à priori. Moreover, thin film growth is strongly affected by experimental conditions.

Theoretical and experimental studies of low coverage overlayers and adsorption sites for overlayer atoms can be used for an educated guess of the in-plane lattice parameter $a$ of thin films. Some experimental papers [5,13,51] report a so-called magic mismatch, where the ratio of the in-plane lattice parameter $a$ of a substrate and of a thin film is approximately equal to a ratio of small integers.

We use this "magic mismatch" as a guidance to select several candidate substrates. We approximate the ratio $a_{\text{bulk}}/a_{\text{sub}}$ by a ratio of small integers, equal it to the ratio of $a_{\text{film}}/a_{\text{sub}}$ and apply the methodology described in Sec. III D to make predictions for corresponding (0001) oriented epitaxial thin films. Thus first we determine the in-plane lattice constant $a_{\text{film}}$ and then the parameters of the film:

$$\frac{a_{\text{bulk}}}{a_{\text{sub}}} \approx \frac{n}{m} = \frac{a_{\text{film}}}{a_{\text{sub}}} \rightarrow a_{\text{film}} \rightarrow c,u$$

with $n, m$ being small natural numbers.

Here we use again the contour plots shown in Figs. 18–20. As the lines for various substrates are very close to each other, we show the details in Fig. 22. Again, we suppose that the equilibrium configuration of the particular film is determined by the total energy minimum along the straight line drawn for that film.

With the help of Fig. 22, we have predicted the parameters of the following films: As on Ti(0001), Co(0001), Zn(0001), and Rh(111) substrates, Sb on C(0001), Zn(0001), Al(111), Ag(111), and Au(111) substrates and Bi on Co(0001), Al(111), Rh(111), Ba(111), and Pb(111) substrates. Their numerical values may be found in Table VI. The substrates were chosen on the basis of minimal absolute value of mismatch and hence it should be easier to prepare the films experimentally.

First, let us compare both LDA and LDA+SOC predictions of the film equilibrium atomic volume $V_{\text{eq}}$ and the internal parameter $u$ obtained using the BAF-cub path with the parameters of the ground state A7 structure. Of course, there is no reason why the lattice parameters of the film should be equal to those of the equilibrium A7 structures, but it is interesting to see the differences.

Thus our values of $V_{\text{eq}}$ for the above mentioned proposed films are smaller by less than 5% when compared to the experimental A7 structure values presented in Table I. Further, the values of both $V_{\text{eq}}$ and $u$ for the films deviate from the equilibrium calculated A7 structural parameters (available in Table III) by less than 2%; deviations of $V_{\text{eq}}$ are both negative or positive.

Let us note that mean values of structural parameters $a$ and $c/a$ corresponding to the experimental data for Bi thin films in Table V lead to relative differences of volume with respect to experimental parameters in Table I less than 7%, the highest deviation occurs in case of Bi/Ge. These differences are comparable with those of our predictions.

TABLE VII. Auxiliary data for drawing the straight lines for various substrates in Figs. 18–20. The Table contains the values of $[c/a](V/V_{\text{exp}}) \times (a(\text{Å}))^3$ at the horizontal boundaries of the contour plots ($V/V_{\text{exp}} = 0.75$ and 1.05).

| $[c/a](V/V_{\text{exp}}) \times (a(\text{Å}))^3$ | As | Sb | Bi |
|---|---|---|---|
| $V/V_{\text{exp}} = 0.75$ | 110.7 | 155.7 | 181.8 |
| $V/V_{\text{exp}} = 1.05$ | 155.0 | 217.9 | 254.5 |

The predicted increase of $u$ agrees with volume dependence of $u$ of the calculated equilibrium A7 structure presented in Table IV. Comparing predictions for different choices of $a$ of the film, we see that $c/3$ and $u$ decrease with increasing $a$ for each element.

Finally, let us discuss a possible influence of a free surface. This represents, of course, a deviation from the bulklike structures considered here. According to Ref. [3], the presence of a free surface on one side of the film does not substantially change the bonding conditions in the film; maximum changes in the lengths of the bonds in the surface layers are less than 8%.

## IV. CONCLUSIONS

We have performed a first-principles study of the total energy of the elements of the 15th group, As, Sb, and Bi, in a three-dimensional parameter space spanned by the A7, bcc, simple cubic (sc) and fcc structures. We have found equilibrium parameters of these four structures and mutual structural energy differences.

It turns out that the LDA+SOC approach gives the best agreement of calculated equilibrium volumes with the experimental data, similarly as in Po [34,39]. Of course, the effect of SOC is much smaller in Sb and As than in Bi. There is a rather general trend of nondecreasing/increasing equilibrium volume per atom in the sequence bcc-fcc-sc-A7.

The fact that the calculations predict bcc structure to be the most compact one with the lowest volume per atom is a natural consequence of the fact that it is so far the last observed structure under increasing pressure at room temperature (see, e.g., summarizing Fig. 1 of Ref. [52]). Moreover, when describing the four structures using the hexagonal parameters, the bcc structure has the lowest $c/a$ ratio, i.e., the (111) atomic planes—forming the bilayers in case of the A7 structure—are the most compressed of all the four structures.

Total energies calculated as functions of the structural parameters $V/V_{\mathrm{exp}}$, $c/a$, and $u$ (where $V/V_{\mathrm{exp}}$ is the atomic volume divided by the experimental value corresponding to the A7 structure, $c/a$ is the ratio of lattice parameters and $u$ is the internal parameter describing nonequidistance of atomic planes along the trigonal axis) were displayed in several contour plots, including their representation at fixed volume, in the $(c/a,u)$ plane, and with $u$ being an appropriately chosen function of $c/a$ so that at least two of the four distinct structures are contained within the plot.

In the $(c/a,u)$ plane, the studied structures correspond to the stationary points of the total energy. Most of them are symmetry-dictated [37,41,53], yet, we have also found some other stationary points which were not dictated by symmetry (see, e.g., Figs. 4, 6, 7, and 23, the last being presented in Appendix B).

We have found that the contour plots of the total energy in the $(V,c/a)$ plane containing bcc, fcc and either sc or A7 structure do not differ significantly when considering three different deformation paths (BSF-lin, BAF-lin, and BAF-cub). Both sc and A7 structures correspond to the total energy minimum in the respective plots and their surrounding is qualitatively very similar.

However, the character of some stationary points may change if we use a different representation of the results. For example, the plot along the linear sc-A7 path (AS-lin) in Fig. 15 shows that the sc structure, corresponding to a minimum on a trigonal deformation path displayed in Fig. 12, becomes a saddle point on this sc-A7 deformation path. This agrees well with the fixed volume deformation path in $(c/a,u)$ plane shown in Fig. 4 that displays the sc structure as a saddle point.

Applying the calculated contour plots to a prediction of the lattice parameters of (0001) epitaxial thin films of A7 structure produced overall good agreement with available experimental data, in particular the combination of BAF-cub path and LDA+SOC approach. Encouraged by the agreement, we have made a plenty of predictions for various substrates presented in Table VI. It would be perhaps easiest to synthesize the films exhibiting the lowest absolute value of mismatch (the fifth column in Table VI) and we recommend them as the first try to the experimentalists willing to approve or disprove the validity of our predictions. Therefore the best candidates would be As/Co(0001), As/Rh(111), Sb/C(0001), Sb/Rh(111), Sb/Al(111), Bi/Ba(111), and Bi/Co(0001).

Figures 18–20 can be used to make further predictions of the bilayer step height $c/3$ and internal parameter $u$ (the latter being a cubic function of $c/a$) or to test the limits of the methods used to obtain the structural parameters by comparing the calculated results with new experimental data. We expect that the results of this work will stimulate further experimental and theoretical studies of these systems.

## ACKNOWLEDGMENTS

This research was supported by by the Ministry of Education, Youth and Sports of the Czech Republic under the Projects CEITEC 2020 (Project No. LQ1601) and Employment of Best Young Scientists for International Cooperation Empowerment (Project No. CZ.1.07/2.3.00/30.0037 co-financed by the European Social Fund and the state budget of the Czech Republic), by the Czech Science Foundation (Project No. GA16-24711S), and by the Academy of Sciences of the Czech Republic (Institutional Project No. RVO:68081723). Computational resources were provided by the Ministry of Education, Youth and Sports of the Czech Republic under the Projects CESNET (Project No. LM2015042), CERIT-Scientific Cloud (Project No. LM2015085), and IT4Innovations National Supercomputer Center (Project No. LM2015070) within the program Projects of Large Research, Development and Innovations Infrastructures. The authors thank P. Lazar for his unpublished pilot calculations used as a benchmark in the early stages of this work.

## APPENDIX A: DETAILED DESCRIPTION OF THE DEFORMATION PATH BAF-CUB

The BAF-cub deformation path $\mathcal{C}$

$$\mathcal{C} = \{(c/a,u)|u(c/a) = a_0 + a_1(c/a) + a_2(c/a)^2 + a_3(c/a)^3\}$$

connecting the bcc, A7, and fcc structures satisfies the restrictions

$$\text{bcc, A7, fcc} \in \mathcal{C},\ \left(\frac{\mathrm{d}\,u(c/a)}{\mathrm{d}\,c/a}\right)((c/a)_{\mathrm{A7}}) = 0.$$

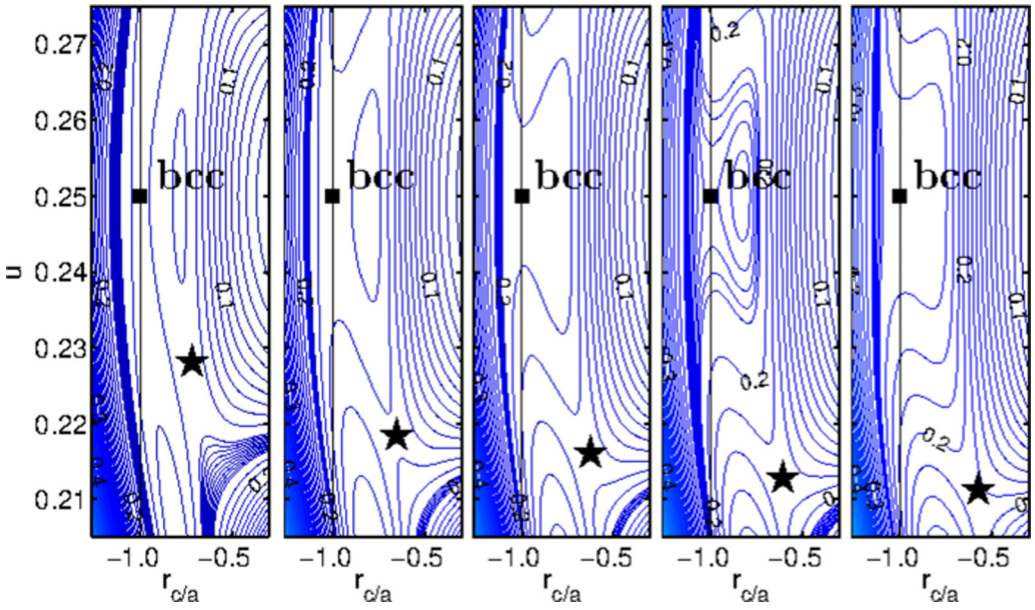


FIG. 23. Details of total energy profiles $E(c/a,u)$ (eV/at) for Bi calculated within the LDA+SOC approach. This set of regions near $r_{c/a} = -1$ (bcc structure) corresponds to $V/V_{\text{exp}}$ equal to 0.958, 0.987, 1.000, 1.020 and 1.040 (left to right). For each segment, the zero of the total energy corresponds to the A7 structure of the segment. The coordinates of the saddle point A7 structures are given in Table IV. Vertical axis is the same for all segments of the plot and its description is given in leftmost segment.

This, together with passing through the three structures, determines all four parameters of a third-order polynomial. The theoretical equilibrium structural parameters obtained within the LDA+SOC approximation (Table III) give the polynomial coefficients presented in Table VIII.

These coefficients were used to determine $u(c/a)$ in the thin film application. Coefficients corresponding to the remaining three approximations are omitted for the sake of brevity. The same applies to the BAF-lin path.

## APPENDIX B: ADDITIONAL INFORMATION ON THE BEHAVIOR OF SADDLE POINTS

Figure 23 shows the volume dependence of position of the saddle point in case of the element Bi. In Table IX, we list the coordinates of the saddle points near the bcc structure in As and Sb as additional data to those presented for the element Bi in Table IV. The volume dependence is qualitatively the same as that of Bi (Fig. 23).

## APPENDIX C: TOTAL ENERGY LANDSCAPE AROUND THE FCC STRUCTURE ("LOBE" STRUCTURE)

From Figs. 24 and 25 showing the total energies of Bi calculated within the LDA and LDA+SOC, we may observe the evolution of the total energy landscape in the neighborhood of the fcc structure as a function of the atomic volume. We can see that with increasing atomic volume the fcc structure becomes more pronounced and the surrounding lobes (neighboring energy minima) move further away from the fcc structure. The appearance of the lobes seems to be shifted to larger volumes when SOC is added. Namely, the total energy profiles of Bi calculated using LDA+SOC (Fig. 25) do not exhibit these lobe-minima until $V/V_{\text{exp}} = 1.00$. Similar tendency has also been observed in case of As ( up to $V/V_{\text{exp}} = 1.00$) and Sb (up to $V/V_{\text{exp}} = 1.02$) but the lobes do not fully evolve when compared to Bi.

TABLE VIII. The coefficients in the description of the BAF-cub deformation paths, $u(c/a)$, in LDA+SOC approximation (see App. A).

| Element | $a_0$ | $a_1$ | $a_2$ | $a_3$ |
|---|---|---|---|---|
| As | 0.310225 | −0.086575 | 0.0291727 | −0.00282328 |
| Sb | 0.297413 | −0.069726 | 0.0249284 | −0.00261503 |
| Bi | 0.299068 | −0.072081 | 0.0256995 | −0.00268649 |

TABLE IX. Coordinates of saddle points corresponding to the A7 structures close to the bcc structure in As and Sb calculated within the LDA and LDA+SOC approach. The corresponding data for Bi are given in the upper part of Table IV.

| | LDA | | | LDA+SOC | | |
|---|---|---|---|---|---|---|
| $V/V_{\text{exp}}$ | $r_{c/a}$ | $c/a$ | $u$ | $r_{c/a}$ | $c/a$ | $u$ |
| | | | As | | | |
| 0.900 | −0.64 | 1.57 | 0.214 | −0.64 | 1.57 | 0.215 |
| 0.940 | −0.60 | 1.62 | 0.212 | −0.60 | 1.62 | 0.211 |
| 0.960 | −0.59 | 1.63 | 0.210 | −0.59 | 1.62 | 0.210 |
| 0.980 | −0.58 | 1.64 | 0.209 | −0.57 | 1.65 | 0.209 |
| 1.000 | −0.54 | 1.68 | 0.208 | −0.54 | 1.68 | 0.208 |
| | | | Sb | | | |
| 0.944 | −0.68 | 1.53 | 0.221 | −0.68 | 1.53 | 0.220 |
| 0.960 | −0.67 | 1.54 | 0.218 | −0.66 | 1.55 | 0.219 |
| 0.977 | −0.65 | 1.56 | 0.218 | −0.65 | 1.56 | 0.217 |
| 1.000 | −0.63 | 1.59 | 0.215 | −0.63 | 1.59 | 0.215 |
| 1.020 | −0.61 | 1.60 | 0.214 | −0.62 | 1.59 | 0.214 |

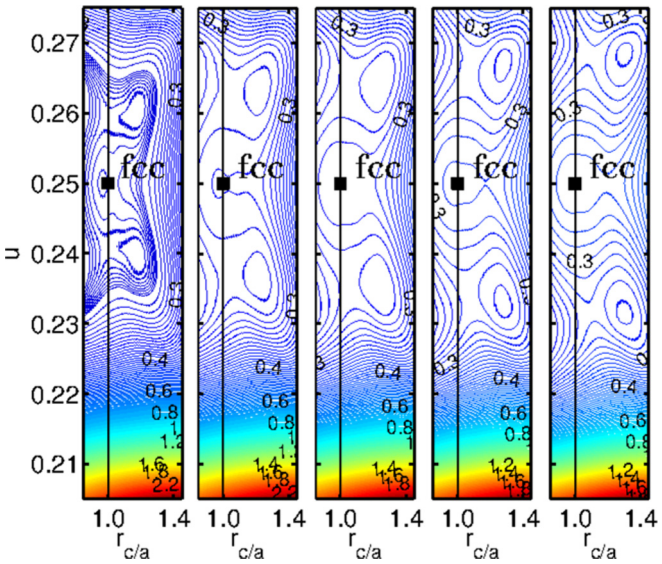


FIG. 24. Total energy profile $E(c/a,u)$ (eV/at) for Bi in the neighborhood of the fcc structure within the LDA (no SOC) at atomic volumes $V/V_{\text{exp}}$ equal to 0.958, 0.987, 1.000, 1.020, and 1.040 (left to right). Total energy minimum for the A7 structure (not shown in the figure) is shifted to zero. The energy difference between neighboring contours is 0.01 eV/atom. Vertical axis is the same for all segments of the plot and its description is given in the leftmost segment.

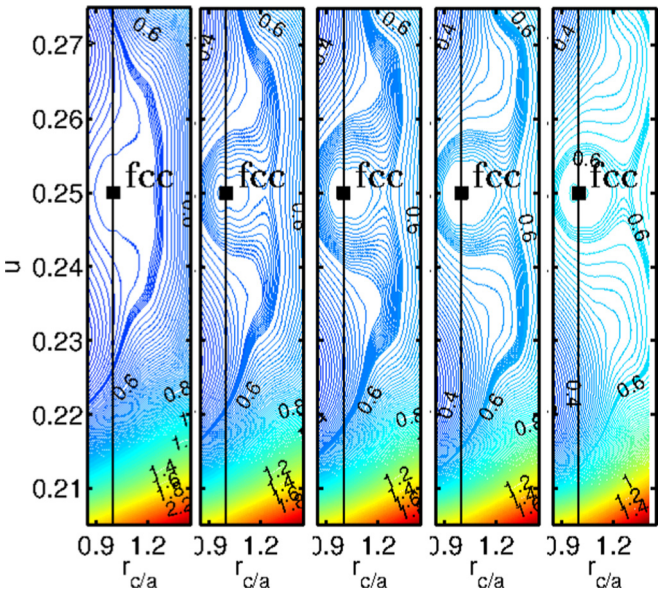


FIG. 26. The same as in Fig. 24 but for As. Total energies are calculated within the LDA for atomic volumes $V/V_{\text{exp}}$ equal to 0.900, 0.940, 0.960, 0.980, and 1.000 (left to right). Vertical axis is the same for all segments of the plot and its description is given in the leftmost segment.

The lobes correspond to local minima of total energy; this is nicely visible especially in case of Bi, LDA, at the highest volumes calculated (Fig. 24). In this particular case, the lobe-minima are present at all calculated volumes. In most parts of Figs. 24 and 25, we have used equidistant contour lines, the step being optimized for simultaneous presentation of the largest portion of the calculated part of the $(c/a,u)$ plane. This choice is somewhat limiting because it may suppress some features in some regions of the calculated $(c/a,u)$ plane. Therefore we have sometimes changed the step manually in some regions in order to improve the presentation.

In case of the other elements, the lobe-minima do not appear, as it may be seen, e.g., in Fig. 4 (Sb) and Fig. 26 (As) nearly for all the volumes calculated, except for higher volumes in Sb treated within the LDA.

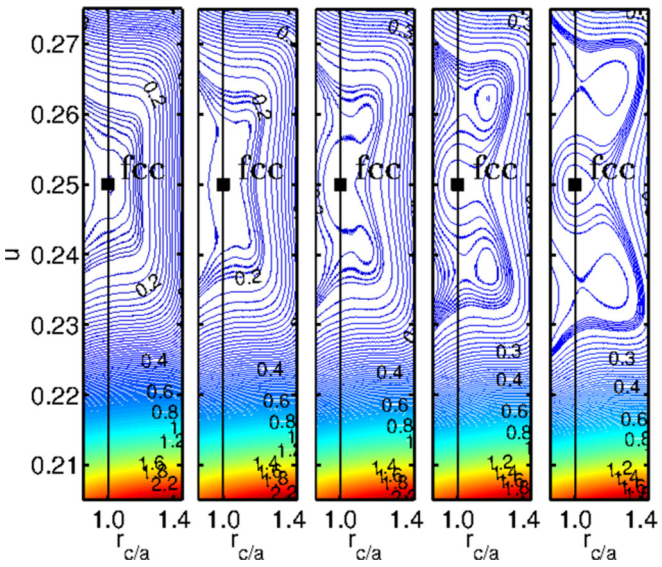


FIG. 25. The same as in Fig. 24 but for the LDA+SOC calculation. Vertical axis is the same for all segments of the plot and its description is given in the leftmost segment.

TABLE X. The results of the test of accuracy of the determination of the values of $c/a$ for thin films from the total energy contour plots for the element Bi. The Table shows the relative differences (in %) between the values of $c/a$ for the bulk A7 structure found from the contour plots along the BAF-lin and BAF-cub paths [denoted as $(c/a)_{\text{plot}}$] and the $c/a$ values directly calculated for the bulk A7 structure [denoted as $(c/a)_{\text{bulk}}$]. The deviation of the $(c/a)_{\text{plot}}$ from the bulk value is described by $(\Delta(c/a))/(c/a) = 100 \times [(c/a)_{\text{plot}}/(c/a)_{\text{bulk}} - 1]$. The GGA+SOC values were not determined as this approach overestimated the equilibrium atomic volume of the A7 structure too much and could not provide any results corresponding well to the experiment.

| | $a$ (Å) | $c/a$ | "predicted" $\frac{\Delta(c/a)}{c/a}$ | |
|---|---|---|---|---|
| Approximation | bulk | bulk | path | value |
| LDA | 4.502 | 2.551 | BAF-lin | −0.2 |
| | | | BAF-cub | 0.1 |
| LDA+SOC | 4.544 | 2.550 | BAF-lin | −0.1 |
| | | | BAF-cub | 0.2 |
| GGA | 4.585 | 2.648 | BAF-lin | −0.8 |
| | | | BAF-cub | −0.2 |

## APPENDIX D: THE RESULTS OF THE BULK TEST OF OUR METHOD FOR DETERMINATION OF PARAMETERS OF THIN FILMS

We have also performed bulk tests in case of Bi. Here we started with the DFT bulk value of $a$ corresponding to the relaxed A7 structure and we used it to "predict" the value of $c/3$, which was compared to the DFT bulk $c/3$ value. This test has been performed for LDA, LDA+SOC and GGA only. The relative difference between the "predicted" and DFT bulk values of $c/3$ is quite small for BAF-lin (less than 1%) and BAF-cub paths (less than 0.2%), as it may be seen from Table X. This test shows that our determination of the value of $c/3$ for the films is quite reliable. The accuracy in determination of $u$ is not worse than 0.8% in all cases studied.

The addition of SOC results in an increase of the equilibrium atomic volume in case of all four structures examined, as it is demonstrated by the values in Table III. As a result, the same tendency occurs for theoretical $c/3$ (and $c/a$) for a given value of $a$ in case of thin films. Moreover, the same order of approximations at increasing equilibrium volume also holds for $c/3$. A small difference between results obtained with the help of BAF-lin and BAF-cub paths is reflected also in a small difference in the thin film results presented in Table V; the corresponding values of $c/3$ from BAF-lin and BAF-cub are very close to each other.


[1] D. Schiferl and C. S. Barrett, J. Appl. Crystallogr. **2**, 30 (1969).
[2] Y. Ren, Z. Qiao, and Q. Niu, Rep. Prog. Phys. **79**, 066501 (2016).
[3] Y. M. Koroteev, G. Bihlmayer, E. V. Chulkov, and S. Blügel, Phys. Rev. B **77**, 045428 (2008).
[4] X. Gonze, J. P. Michenaud, and J. P. Vigneron, Phys. Scr. **37**, 785 (1988).
[5] T. Shirasawa, M. Ohyama, W. Voegeli, and T. Takahashi, Phys. Rev. B **84**, 075411 (2011).
[6] S. Yaginuma, K. Nagaoka, T. Nagao, G. Bihlmayer, Y. M. Koroteev, E. V. Chulkov, and T. Nakayama, J. Phys. Soc. Jpn. **77**, 014701 (2008).
[7] A. I. Oreshkin, J. T. Sadowski, T. Nagao, S. Yaginuma, Y. Fujikawa, T. Sakurai, and T. Ohno, Int. J. Nanosci. **6**, 399 (2007).
[8] S. Yaginuma, T. Nagao, J. T. Sadowski, M. Saito, K. Nagaoka, Y. Fujikawa, T. Sakurai, and T. Nakayama, Surf. Sci. **601**, 3593 (2007).
[9] C. Bobisch, A. Bannani, M. Matena, and R. Moeller, Nanotechnology **18**, 055606 (2007).
[10] T. Romann, E. Anderson, S. Kallip, H. Maendar, L. Matisen, and E. Lust, Thin Solid Films **518**, 3690 (2010).
[11] G. Jnawali, H. Hattab, B. Krenzer, and M. H. von Hoegen, Phys. Rev. B **74**, 195340 (2006).
[12] T. Nagao, J. T. Sadowski, M. Saito, S. Yaginuma, Y. Fujikawa, T. Kogure, T. Ohno, Y. Hasegawa, S. Hasegawa, and T. Sakurai, Phys. Rev. Lett. **93**, 105501 (2004).
[13] S. Hatta, Y. Ohtsubo, S. Miyamoto, H. Okuyama, and T. Aruga, Appl. Surf. Sci. **256**, 1252 (2009).
[14] J. Yuhara, M. Yokoyama, and T. Matsui, J. Appl. Phys. **110**, 074314 (2011).
[15] T. Payer, I. Rajkovic, M. Ligges, D. von der Linde, M. H. von Hoegen, and F.-J. M. zu Heringdorf, Appl. Phys. Lett. **93**, 093102 (2008).
[16] M. Kammler and M. H. von Hoegen, Surf. Sci. **576**, 56 (2005).
[17] H. J. Beister, K. Strossner, and K. Syassen, Phys. Rev. B **41**, 5535 (1990).
[18] C. R. S. da Silva and R. M. Wentzcovitch, Comput. Mater. Sci. **8**, 219 (1997).
[19] M. Durandurdu, Phys. Rev. B **72**, 073208 (2005).
[20] W. Feng, S. Cui, H. Hu, and H. Liu, Physica B **400**, 22 (2007).
[21] P. Silas, J. R. Yates, and P. D. Haynes, Phys. Rev. B **78**, 174101 (2008).
[22] N. Huntemann, E. S. Zijlstra, and M. E. Garcia, Appl. Phys. A **96**, 19 (2009).
[23] H. Iwasaki and T. Kikegawa, Acta Crystallogr. **53**, 353 (1997).
[24] O. Degtyareva, M. I. McMahon, and R. J. Nelmes, High Press. Res. **24**, 319 (2004).
[25] K. Aoki, S. Fujiwara, and M. Kusakabe, J. Phys. Soc. Jpn. **51**, 3826 (1982).
[26] U. Haussermann, K. Soderberg, and R. Norrestarrit, J. Am. Chem. Soc. **124**, 15359 (2002).
[27] H. Katzke and P. Toledano, Phys. Rev. B **77**, 024109 (2008).
[28] M. I. McMahon and R. J. Nelmes, Chem. Soc. Rev. **35**, 943 (2006).
[29] Y. Liu and R. E. Allen, Phys. Rev. B **52**, 1566 (1995).
[30] M. Friák, M. Šob, and V. Vitek, Phys. Rev. B **63**, 052405 (2001).
[31] M. Zelený and M. Šob, Phys. Rev. B **77**, 155435 (2008).
[32] M. Zelený, D. Legut, and M. Šob, Phys. Rev. B **78**, 224105 (2008).
[33] J. Donohue, *Structures of the Elements* (Wiley, Hoboken, New Jersey, 1974).
[34] D. Legut, M. Friák, and M. Šob, Phys. Rev. B **81**, 214118 (2010).
[35] *Smithells Metals Reference Book*, edited by W. F. Gale and T. C. Totemeier (Butterworth-Heinemann, Oxford, 2004), pp. 6–30 and 6–31.
[36] Z. Yan, S. S. Kushvaha, W. Xiao, and X.-S. Wang, Appl. Phys. A **88**, 299 (2007).
[37] M. Šob, L. G. Wang, and V. Vitek, Comput. Mater. Sci. **8**, 100 (1997).
[38] M. Šob, L. G. Wang, and V. Vitek, Mater. Sci. Eng. A **234-236**, 1075 (1997).
[39] D. Legut, M. Friák, and M. Šob, Phys. Rev. Lett. **99**, 016402 (2007).
[40] M. Zelený, M. Friák, and M. Šob, Phys. Rev. B **83**, 184424 (2011).
[41] P. J. Craievich, M. Weinert, J. M. Sanchez, and R. E. Watson, Phys. Rev. Lett. **72**, 3076 (1994).
[42] P. E. Blöchl, Phys. Rev. B **50**, 17953 (1994).
[43] G. Kresse and D. Joubert, Phys. Rev. B **59**, 1758 (1999).
[44] D. M. Ceperley and B. J. Alder, Phys. Rev. Lett. **45**, 566 (1980).
[45] J. P. Perdew, J. A. Chevary, S. H. Vosko, K. A. Jackson, M. R. Pederson, D. J. Singh, and C. Fiolhais, Phys. Rev. B **46**, 6671 (1992).
[46] K. Albe, K. Nordlund, J. Nord, and A. Kuronen, Phys. Rev. B **66**, 035205 (2002).
[47] X. Wang, K. Kunc, I. Loa, U. Schwarz, and K. Syassen, Phys. Rev. B **74**, 134305 (2006).

[48] L. E. Diaz-Sanchez, A. H. Romero, and X. Gonze, Phys. Rev. B **76**, 104302 (2007).
[49] K. Seifert, J. Hafner, J. Furthmüller, and G. Kresse, J. Phys. Condens. Matter **7**, 3683 (1995).
[50] D. Mukherjee, B. D. Sahoo, K. D. Joshi, and S. C. Gupta, J. Appl. Phys. **115**, 053702 (2014).
[51] T. Payer, C. Klein, M. Acet, V. Ney, M. Kammler, F.-J. M. zu Heringdorf, and M. H. von Hoegen, Thin Solid Films **520**, 6905 (2012).
[52] U. Haussermann, Chem. Eur. J. **9**, 1471 (2003).
[53] P. J. Craievich, J. M. Sanchez, R. E. Watson, and M. Weinert, Phys. Rev. B **55**, 787 (1997).